Few-Shot Learning for Industrial Time Series: A Comparative Analysis Using the Example of Screw-Fastening Process Monitoring

Xinyuan Tu[1] xinyuan.tu@fau.de
Haocheng Zhang[1] maxzhang@fau.de
Tao Chengxu[1] chengtao.xu@fau.de
Zuyi Chen[1] zuyi.chen@fau.de

[1]Friedrich-Alexander-Universität Erlangen-Nürnberg

*Corresponding author: Xinyuan Tu

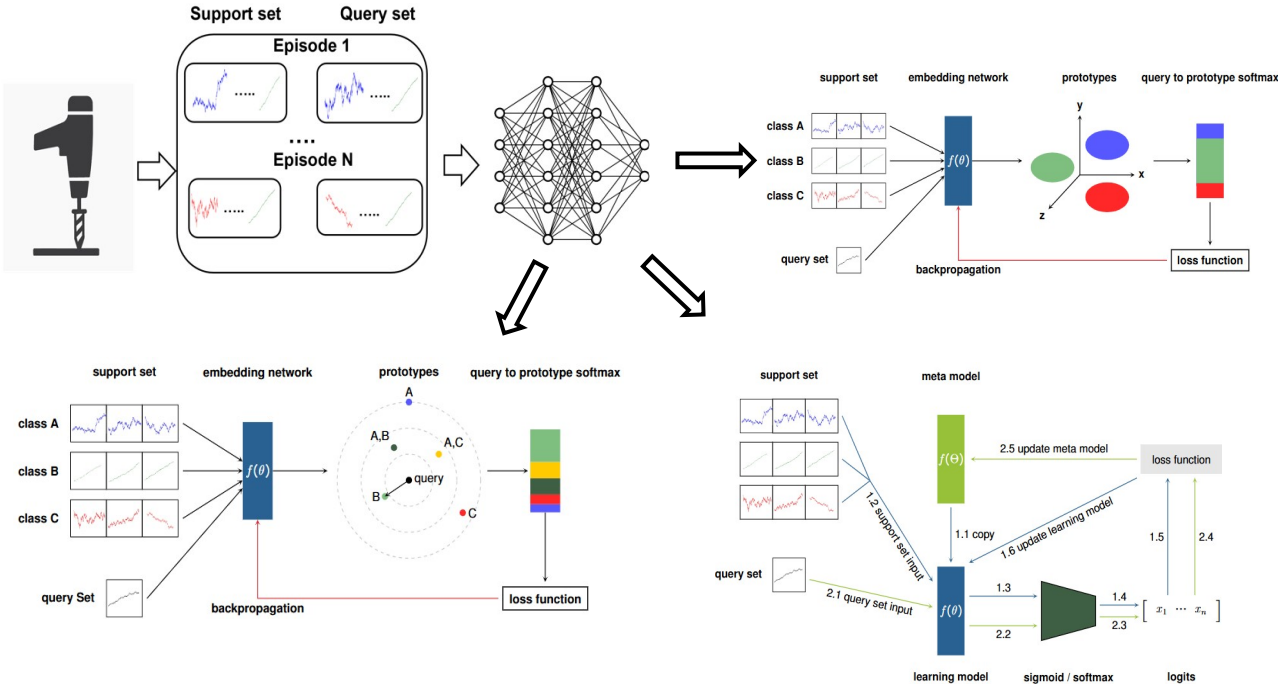

Abstract

Few–shot learning (FSL) has shown promise in vision but remains largely unexplored for *industrial* time-series data, where annotating every new defect is prohibitively expensive. We present a systematic FSL study on screw-fastening process monitoring, using a 2 300-sample multivariate torque dataset that covers 16 uni- and multi-factorial defect types. Beyond benchmarking, we introduce a **label-aware episodic sampler** that collapses multi-label sequences into multiple single-label tasks, keeping the output dimensionality fixed while preserving combinatorial label.

Two FSL paradigms are investigated: the metric-based *Prototypical Network* and the gradient-based *Model-Agnostic Meta-Learning* (MAML), each paired with three backbones—1D CNN, InceptionTime and the 341 M-parameter transformer *Moment*. On 10-shot, 3-way evaluation, the InceptionTime + Prototypical Network combination achieves a **0.944 weighted F1** in the multi-class regime and **0.935** in the multi-label outperforming finetuned Moment by up to 5.3 % while requiring two orders of magnitude fewer parameters and training time. Across all backbones, metric learning consistently surpasses MAML, and our label-aware sampling yields an additional 1.7% F1 over traditional class-based sampling.

These findings challenge the assumption that large foundation models are always superior: when data are scarce, lightweight CNN architectures augmented with simple metric learning not only converge faster but also generalize better. We release code, data splits and pre-trained weights to foster reproducible research and to catalyze the adoption of FSL in high-value manufacturing inspection.

Contents

List of Figures

List of Tables

List of Abbreviations

1D CNN	One Dimensional Convolution Neural Network
EEG	Electroencephalography
FSL	Few-Shot Learning
HST	High-Speed-Train
Lora	Low-Rank Adaptation of Large Language Models
MAML	Model-Agnostic Meta-Learning
TSML	Task-Sequencing Meta Learning

1 Introduction and Objective

Supervised learning models have demonstrated remarkable success across various domains, from computer vision and time series to natural language processing [8]. However, most supervised learning models often require large-scale labeled datasets to achieve high performance [9]. This quite limits their applicability in scenarios where labeled data is inadequate.

Few-Shot Learning (FSL) aims to address this challenge by enabling models to generalize effectively from only a handful of training examples [10]. Few-shot learning has gained significant attention due to its potential to learn from a very limited data, where new concepts can be understood with minimal exposure [10]. Recent advancements [11, 12, 13, 14, 15] in few-shot learning have explored meta learning frameworks optimization-based approaches (e.g.Model-Agnostic Meta-Learning (MAML) [1]) and metric-learning techniques like Prototypical Networks [16] and Siamese Networks [17]. Additionally, large-scale pretrained foundation models, particularly transformer-based architectures, have demonstrated impressive few-shot capacities [18, 19].

FSL in time-series data remains underexplored, with only a limited number of studies published. Addressing these challenges could bring significant benefits to the engineering industry, as in some cases there are very limited samples of defects [20]. For instance, an industrial report from Sweden highlights the substantial economic impact of defects in construction, noting that preventing rare defects can save up to 18% of the total cost [21].

In this study, we provides an in-depth exploration of few-shot learning within the engineering domain—focusing on time-series data from screw-fastening process monitoring—and evaluates its performance across a range of methodologies. To address the scarcity of labeled screw fastening datasets, we employ rigorous data preprocessing techniques followed by effective episodic sampling approaches. We evaluate existing few-shot learning methods tailored for time-series tasks, assess their effectiveness, and discuss key challenges associated with few-shot learning in screw-fastening process datasets. Chapter 2 reviews the fundamentals and related work in FSL and time-series classification. In chapter 3, we introduce our screw-fastening dataset and describe its collection process. Chapter 4 presents the preprocessing techniques applied to the data. In chapter 5, we detail our implementations and examine the various methodologies. Chapter 6 outlines the experimental setup and results. Finally, we offer perspectives on enhancing the performance and generalization of FSL models for industrial time-series classification.

2 Relevant Fundamentals and Related Work

This chapter provides an overview of the fundamental concepts and related research essential for understanding FSL and time series classification. It begins with a discussion on traditional supervised learning and its limitations in data-scarce scenarios, followed by the definition and key principles of few-shot learning. Additionally, the chapter introduces time series data and its unique characteristics. The subsequent sections explore existing studies on FSL, various learning models, and notable neural network architectures applied in time series classification.

2.1 Relevant Fundamentals

2.1.1 Traditional Supervised Learning

Traditional supervised learning is a learning paradigm in which a model is trained on a dataset of input-output pairs [22]. Given a training set $\mathcal{D}_{train} = \{(x_i, y_i)\}_{i=1}^{N}$ of size N, the objective is to learn a function f from input feature to output by minimizing a loss $\mathcal{L}$. $\mathcal{L}$ can be defined as [23]:

$$\mathcal{L}(\theta) = \frac{1}{N} \sum_{i=1}^{N} L\big(y_i, f(x_i; \theta)\big) \tag{2.1}$$

where L is a loss function (e.g., cross-entropy for classification or mean squared error for regression). The model is then evaluated on unseen data $\mathcal{D}_{test} = \{(x_j, y_j)\}_{i=N+1}^{N+M}$ to assess its generalization ability [24]:

$$y_j \approx f(x_j; \theta^*) \text{ for } (x_j, y_j) \in \mathcal{D}_{test} \tag{2.2}$$

and

$$\theta^* = \arg\min_{\theta} \mathcal{L}(\theta) \tag{2.3}$$

2.1.2 FSL

FSL builds upon the framework of traditional supervised learning but addresses scenarios where only a very limited number of examples per class is available [10]. The dataset is composed of episodes. Each episode τ_i consists of a support set S_{τ_i} and a query set Q_{τ_i} [24]. Support set S_{τ_i} is an N-ways-K-shots dataset, and query set Q_{τ_i} is an N-ways-M-shots dataset. Each S_{τ_i} and Q_{τ_i} has no intersection but have the same label space [24]:

$$S_{\tau_i} \cap Q_{\tau_i} = \varnothing \tag{2.4}$$
$$Y = \{y \mid (x, y) \in Q_{\tau_i}\} \tag{2.5}$$
$$Y' = \{y \mid (x, y) \in S_{\tau_i}\} \tag{2.6}$$
$$Y = Y' \tag{2.7}$$
$$|Y| = |Y'| = N \tag{2.8}$$
$$|S_{\tau_i}| = K \times N \tag{2.9}$$
$$|Q_{\tau_i}| = M \times N \tag{2.10}$$

where:

- K denotes the number of examples per class (K shots) in support set.
- M denotes the number of examples per class (M shots) in query set.
- N denotes the number of classes (N ways).
- x denotes the input features.
- $y \in \{0, 1, \ldots, C-1\}$ denotes the class label, where C is number of classes in the dataset.

Assume we have a list of episodes as training set $\mathcal{T}_{train} = \{\ldots \tau_i \ldots\}$. The objective is to learn a function from each support set S_{τ_i} and query set Q_{τ_i} from the training episodes [24]. The loss function for one training episode τ_i is defined as [24]:

$$\mathcal{L}_{\tau_i}(\theta) = \frac{1}{M} \sum_{(x,y) \in Q_{\tau_i}} L\big(y, f(x; \theta, S_{\tau_i})\big), \tag{2.11}$$

where $f(x; \theta, S_{\tau_i})$ denotes the model learned from support set S_{τ_i}, and L is the loss function, e.g. cross entropy.

Similarly to the traditional supervised learning, the model is evaluated on unseen episodes $\mathcal{T}_{test}$. For each test episode $\tau_i \in \mathcal{T}_{\text{test}}$ and each sample $(x, y) \in Q_{\tau_i}$, the objective is that the model f approximates the ground truth [24]:

$$y \approx f(x; \theta^*, S_{\tau_i}) \tag{2.12}$$

where:

$$\theta^* = \arg\min_{\theta} \mathbb{E}_{\tau_j \in \mathcal{T}_{train}} \mathcal{L}_{\tau_j}(\theta) \tag{2.13}$$

Episode Sampling Episode sampling is a fundamental process in FSL. It is designed to structure training in a way that closely resembles the few-shot scenario. Each episode consists of a support set and a query set, both drawn from a subset of available classes. For multi-class data, though we didn't find its formal definition, we could infer from Parnami and Lee [24, p. 9]. It first samples N-way classes uniformly without replacement. Then it samples the support set and query set uniformly from the selected classes. Specially, it would be uniformly selecting $K \times N$ samples and $M \times N$ for the support set and query set, respectively. For the multi-label situation, Liang et al. [25] discuss the episodic construction. However, it's not applied in this report because of its complexity and non-existing source code. We propose our own multi-label

episodic sampling method in chapter 4.

Meta Learning Meta learning [26, 27] or Learning to Learn [28] explores the meta learning abilities of models. Inspired by theories of human development, meta learning aims to extract useful priors from past experiences to accelerate learning on future tasks. Whereas a conventional model tackles one classification problem at a time, a meta learner acquires a generalized strategy for classification by training across many related tasks. As a result, when faced with a new but analogous challenge, the meta learner can adapt rapidly and effectively. [24]

In this report, all of our FSL methodologies employ meta-learning techniques—both metric- and optimization-based (see Chapter 2.1.2) but are researched under FSL framework. Therefore, to avoid complicating the readers and introducing inconvenience, we will not dive further into the concepts of meta learning. Introduction on FSL concepts are sufficient for this project.

FSL models There are mainly four types of FSL models [24]:

- *Metric-based* [29] approaches learn a representation in which classification reduces to measuring the distance between a query point and class prototypes. [24]
- *Optimization-based* (gradient-based) approaches learns either an initialization or an inner-loop update rule so that only a few gradient steps with the support data suffice to obtain a task-specific model. [24]
- *Model-based* approaches equip the learner with rapidly updatable internal or external memories which allows to quickly encode and retrieve new information and can potentially obviate the downsides of conventional models. [30]
- *Transfer learning* [31] is a non-meta learning approach that improves learning in the target domain by leveraging knowledge from the source domain, usually cooperated by using a pretrained network from the source task. One naive example is using a pretrained network, then finetuning it on support set and then inference on query set. [24]

Prototypical Network Prototypical network [16] is a widely used metric-based approach for FSL. The model learns an embedding space in which each class is represented by a prototype, computed as the mean of the support set examples in that representation space [16]. Classification is performed by computing the distance between a query point and the class prototypes [16]. This approach has been highly effective in few-shot classification tasks due to its simplicity and efficiency [32, 33]. Figure 1 shows an example of Prototypical network handling support set and query set. The prototypes are formed by computing the mean of class A, B and C in representation space. Afterwards, the class probability of the query set is obtained by using Softmax with the negative value of the distance from its representation vector to centroid A, B and C respectively.

Model-Agnostic Meta-Learning Model-Agnostic Meta-Learning (MAML) [1] takes an optimization-based approach by learning an initialization that enables rapid adaptation to new episodes. Instead of learning a fixed embedding, MAML trains a model across a distribution of episodes such that only a few gradient updates are needed for generalization. This approach allows model learning how to adapt itself to different episodes and learning to learn. [1]

One illustration can be found in Figure 2, where the meta learner learns to adapt to episodes, resulting in weights θ_1, θ_2 and θ_3 respectively.

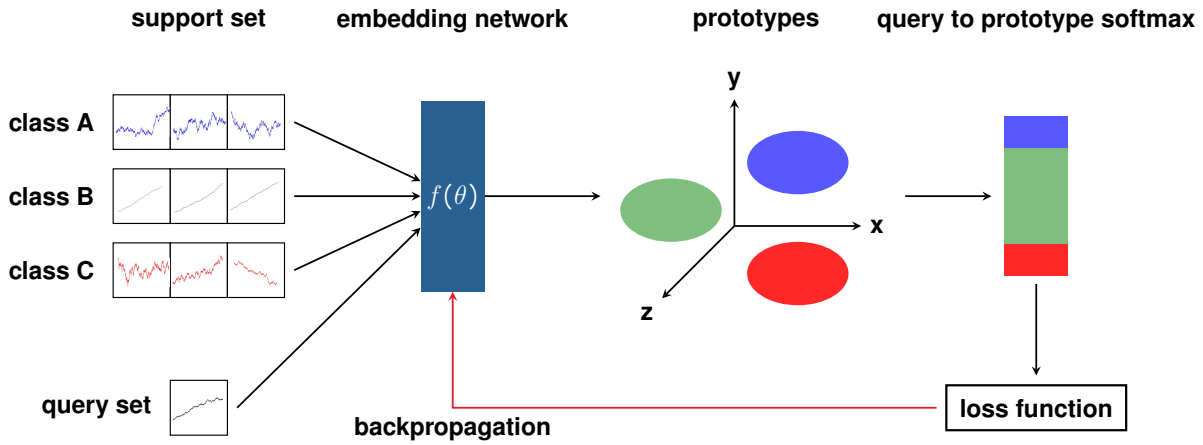

Figure 1: One example of prototypical network handling a support set with N-way=3 and N-shot=3. The query set is simplified to have one sample.

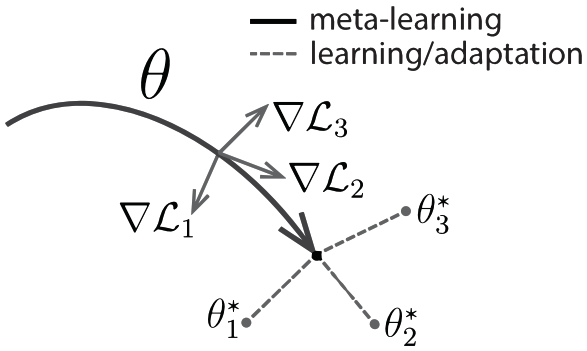

Figure 2: One example that MAML adapts to different episodes [1]

2.1.3 Time Series Classification

Time series classification is the task of assigning a discrete label to an entire sequence of observations collected over time [34]. Let a time series of variables $D \geq 1$ and length T be represented as [34]:

$$X = (x_1, x_2, \ldots, x_T) \in \mathcal{R}^{T \times D}, \tag{2.14}$$

where x_t denotes the observation at time t and T is the length of the time series. If $D = 1$, the time series is called univariate time series. Otherwise, it's a multivariate time series. Given a dataset of labeled time series $\mathcal{D} = \{(X_i, y_i)\}_{i=1}^{N}$, the goal is to learn a classifier f such that for an unseen time series X', the predicted label $f(X'; \theta)$ approximates the true label y_i.[34]

1D CNN Recent research in time series classification has increasingly leveraged One Dimensional Convolution Neural Network (1D CNN) due to its ability to capture local temporal patterns and extract hierarchical features directly from raw sequential data. A typical 1D CNN for time series classification processes raw sequential data through a series of convolution layers with sliding filters that extract local temporal features, interleaved with non-linear activations and pooling layers to reduce dimensionality and achieve invariance. Finally, the network aggregates these features—often via global pooling—and feeds them into fully connected layers

that produce the final class probabilities. [34]

InceptionTime InceptionTime [2] is a state-of-the-art time series architecture. Similar to how AlexNet [35] transforms image classification by learning hierarchical representations, InceptionTime consists of Inception Modules and allows several parallel convolutional filters with different kernel sizes to capture temporal features at multiple scales, as shown in Figure 3. InceptionTime has performed excellently in some open public time series dataset. [2]

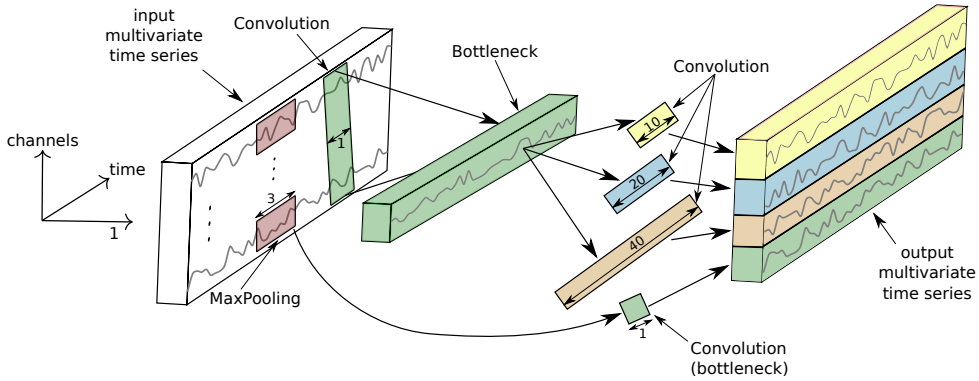

Figure 3: Structure of Inception module [2]

Moment In the time series domain, several transformer-based foundation models have emerged. One of the examples is Moment [3], a family of open-source foundation models. It is pretrained on 27 datasets across 13 domains, from healthcare, power, electricity to gait. To capture the rich and diverse patterns present in time series data, Moment adopts an architecture inspired by large language models. As shown in Figure 4, the overall design includes patching, transformer encoder and reconstruction head. Depending on the specific task, the model dynamically adapts its behavior and processing pipeline. Moment has performed great in some public time series benchmarks. [3]

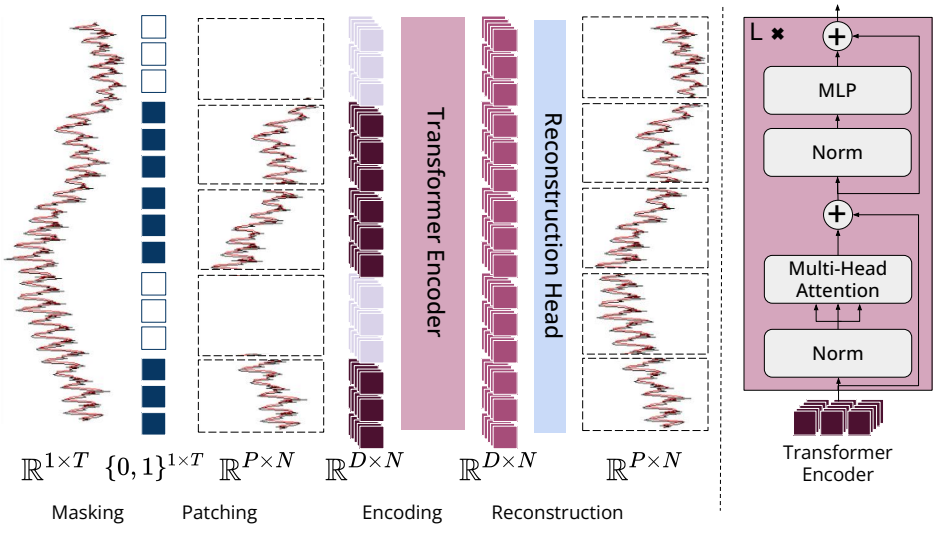

Figure 4: Overview of Moment [3]

2.2 Related Work

Wu and Chan [36] integrate Reptile [37] with compact convolutional layers and evaluate it on Electroencephalography (EEG) datasets—BCI-IV 2a [38] and PhysionetMI [39]. Their results demonstrate that Reptile can improve EEG few-shot motor classification. Wang et al. [40] leverage Matching network [41] with a 1D-CNN: an EEG segment and a reference waveform are projected into a shared embedding space, and their cosine similarity is computed. Sun et al. [42] applies Prototypical network [16] with a lightweight 1D-CNN to obtain latent representations. Once the entire support set is processed and prototypes are formed, a module called **Prototype Enhancement**, consisting of a multi-head self-attention layer, enables prototypes to "look at others," thereby becoming more discriminative. When the query set is provided, the model predicts by measuring the distance between the query and the prototypes in the representation space. Papaioannou et al. [43] propose the label-combinational prototypical network, which extends the vanilla prototypical network to the multi-label regime and employs a lightweight VGGish [44] backbone. The label-combinational prototypical network shows strong performance on world-music-tagging benchmarks [45, 46, 47, 48, 49]. Tam et al. [50] employ a Siamese network structure [17] consisting of a single 2D CNN with three convolution blocks (kernel 3×3, ReLU, BN, MaxPool). Prediction is based on the cosine similarity between the query set and the support set in latent space. The method shows good performance on a private hand-gesture EMG dataset. Rahimian et al. [51] develop a framework called FS-HGR, which treats the N-way K-shot task as a sequence-to-sequence meta-learning problem. Each episode sequence comprises the K labeled support samples and several query samples; the network is expected to predict the labels of the query samples after being provided with the labeled support set, like SNAIL [52]. The network involves several Temporal Convolutional Network layers, several multi-head attention layers, and a fully connected layer. FS-HGR demonstrates moderate performance on Ninapro Database 2 [53]. Zhang et al. [54] try MAML with two different backbones, a 1D CNN and an LSTM. They train MAML [1] on high-frequency diseases, e.g. Amnesia, Parkinson's, and Dementia, and evaluate it on Alzheimer's, a rare disease. Hu et al. [55] propose Task-Sequencing Meta Learning (TSML), where episodes are ranked from easy to hard to enable the network to learn from the easier ones first. A k-means algorithm clusters the support set in each episode. Each episode is ranked based on the accuracy of samples in the support set when k-means converges. The model performs well on the private Farop dataset. Wang et al. [56] incorporate self supervised learning with a Siamese network. They select small proportions of the dataset, the CWRU bearing dataset [57] and the High-Speed-Train (HST) wheel-set bearing dataset [58], for self supervised learning. The self supervised task involves classifying six transformations (original, time-reverse, random-increase, random-reduction, set-zero, add-noise). Once the self supervised task is complete, the pretrained weights are transferred to initialize the backbone of the Siamese network. The results showed a good performance.

Table 1 summarizes the related work. It can be observed that most of the related works focus on biomedical domain, and there are few working in industrial times series. Furthermore, most of the related work is based on simple architectures or their variants. For FSL methodologies, metrics-based learning (Prototypical network, Matching network, Siamese network) are mostly preferred while few prefer optimization-based (MAML, Reptile) and model-based (SNAIL). Most of domain datasets are structured in multi-class except Papaioannou et al. [43] adapt FSL methodology into multi-label.

Table 1: Related work summarization. Abbreviations used in this table: EEG (Electroencephalography), EMG (Electromyography), EHR (Electronic Health Record), TCN (Temporal Convolutional Network).

Literature	Domain	Dataset	Methodology	Backbone
Wu and Chan [36]	EEG	BCI-IV 2a [38] PhysionetMI [39]	Reptile [37]	CNN
Wang et al. [40]	EEG	Benchmark [59] BETA [60]	Matching network [41]	TCN
Sun et al. [42]	EEG	Mit-BIH [61] FaceAll [62] UWave [62]	Prototypical network [16]	CNN
Papaioannou et al. [43]	Audio	[45], [46], [47], [48], [49]	Prototypical network	VGGish [44]
Tam et al. [50]	EMG	Private hand gesture EMG	Siamese network [17]	CNN
Rahimian et al. [51]	EMG	Ninapro DB-2 [53]	SNAIL [52]	TCN and multi-head attention
Zhang et al. [54]	EHR	private heath records	MAML [1]	CNN / LSTM
Hu et al. [55]	Industrial time series	Farop (private)	MAML	VGG-11 [63] Resnet-18 [64]
Wang et al. [56]	Industrial time series	CWRU [57] HST wheel-set [58]	Siamese network	CNN

3 Use Case Description and Data Understanding

In this chapter, we describe the data source, including details about how the raw data was collected and the nature of the information it contains. Next, we proceed to data understanding, examining the dataset from a data science perspective. We explore the data thoroughly, aiming to identify key characteristics, uncover potential insights, and recognize inherent limitations or challenges. Finally, we discuss how this raw dataset can support our project's specific research objectives.

3.1 Data Source

The M6 screw-fastening time series is collected by Songsik [4] and further reconstructed by Paulus [65] at Friedrich Alexander University Erlangen. The screw-fastening data was collected using a DEPRAG screwdriver (model 320EWT27-0035-F6 from the MINIMAT-EC series [66]) featuring an interchangeable internal hexagon screwdriver bit. Fastening was initiated by activating a lever and concluded upon lever release or reaching a predefined torque limit. The status of each fastening was indicated via an LED display: green represented "in order (i.O.)", and red indicated "not in order (n.i.O.)" [4]. Torque data was precisely recorded through motor current measurements.

The process was controlled by a DEPRAG AST11-1/-S system, operated via a web-based PC interface. The main tightening method was torque-controlled ("Verschrauben/Lösen auf Drehmoment"), which is common in industrial applications. Before every tightening, the operator install either a fault-free setup or a specific fault (or fault combination), so the true class was known. That class ID (e.g. `class24`) was written into the CSV filename and later parsed as the label [4]. Figure 5 shows the collection overview.

Figure 5: Overview of data collection [4]

3.2 Data Understanding

As discussed in the data source section, the dataset was collected using a high-precision screwdriver. During each screw-driving session, the screwdriver periodically recorded torque values and other relevant physical quantities, which results in a time series for each sample. In total, 2,300 samples were obtained, each of which captures the dynamics of the screwing process over time. Each sample is structured as a multivariate time series with six fields, as outlined in Table 2. The fields include time, rotational speed, torque, angle, program step, and current.

Table 2: Raw data structure [4]

Field	Description
time (0.001 ms)	time at which measurement is recorded.
rotational speed (RPM)	screw's rotational speed in revolutions per minute.
torque (N·m)	amount of torque being applied during the process.
angle (°)	rotational angle of the screw or part.
program step	current step in the programmed sequence.
current (A)	electric current drawn by the motor or system.

The collected dataset spans 16 different categories, including seven uni-factorial defect types, seven multi-factorial defect types and one normal type, as shown in Table 3. The class labeled ”0 in order” represents the standard and defect-free samples.

Table 3: Collected sample overview for each class [4]

Class	Count	Label Representation
0 in order	200	[0,0,0,0,0,0,0]
1 small through bore	200	[1,0,0,0,0,0,0]
2 offset joint partners	200	[0,1,0,0,0,0,0]
3 uneven joint area	200	[0,0,1,0,0,0,0]
4 span in the thread	200	[0,0,0,1,0,0,0]
5 dirty screw	200	[0,0,0,0,1,0,0]
6 foreign body at the end of the thread	200	[0,0,0,0,0,1,0]
7 damaged screw	200	[0,0,0,0,0,0,1]
class 16	100	[1,0,0,0,0,1,0]
class 24	100	[0,1,0,1,0,0,0]
class 27	100	[0,1,0,0,0,0,1]
class 35	100	[0,0,1,0,1,0,0]
class 37	100	[0,0,1,0,0,0,1]
class 267	100	[0,1,0,0,0,1,1]
class 357	100	[0,0,1,0,1,0,1]
total	2300	

To better understand the torque behavior across these different classes, we visualized each

class's average torque value over time in Figure 7 and Figure 6. In this figure, the x-axis represents time in seconds, while the y-axis shows torque in Newton meters (N·m). This visualization highlights the distinction between each class.

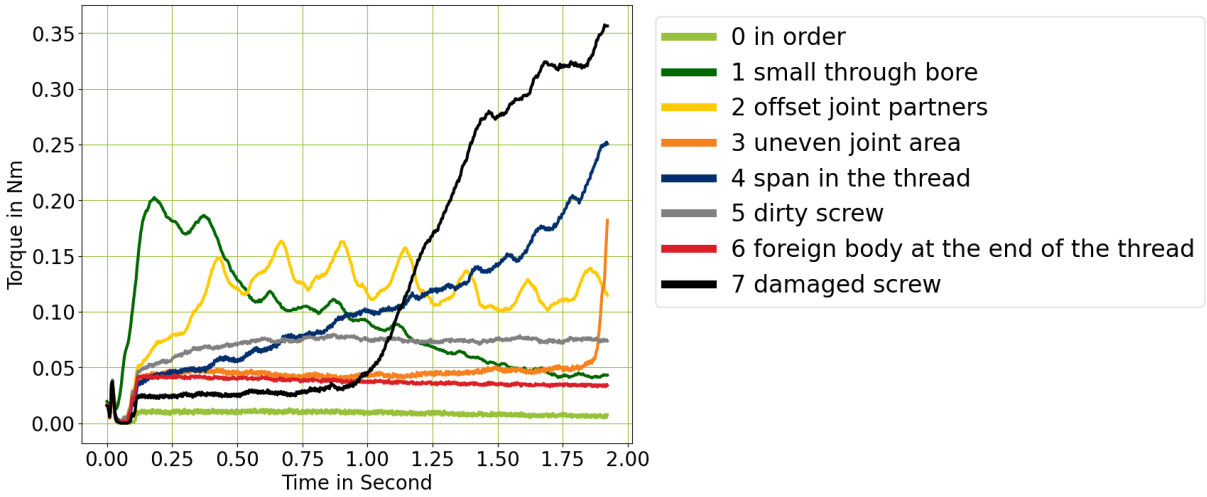

Figure 6: Data overview averaged by each single-labeled samples. The y-axis shows the torque value in Newton meters, and the x-axis is the time in seconds.

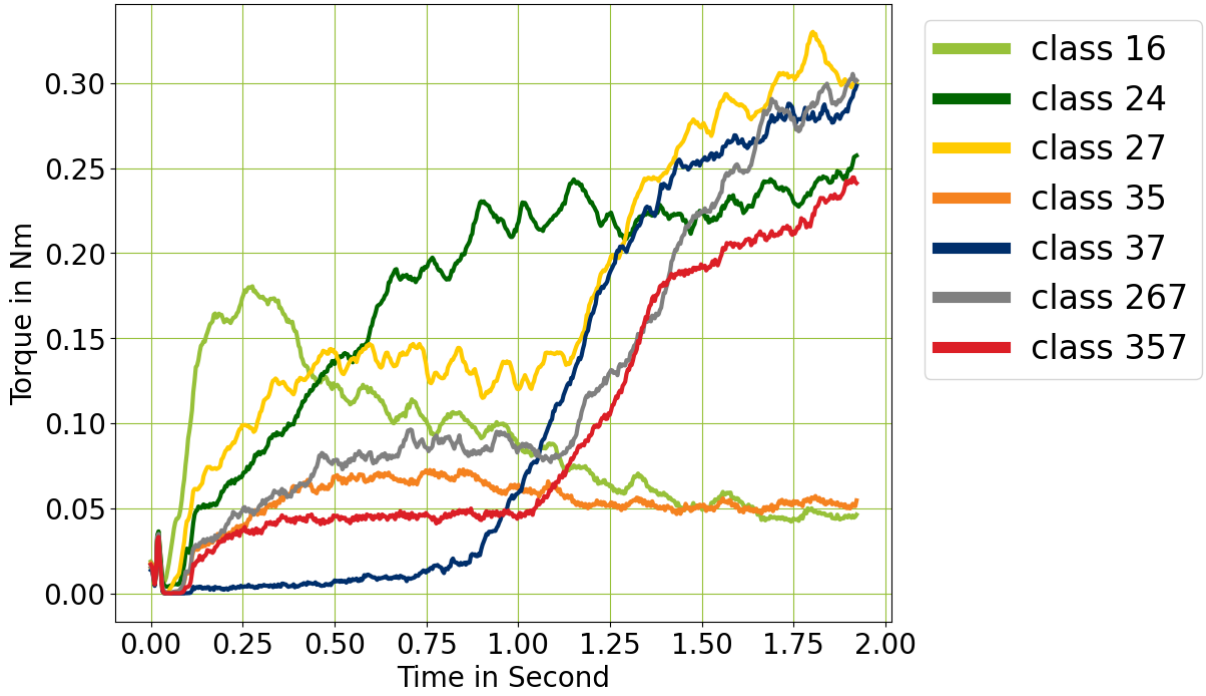

Figure 7: Data overview averaged by each multi-labeled samples. The y-axis shows the torque value in Newton meters, and the x-axis is the time in seconds.

3.3 Use Case Description

Our use case addresses real-world manufacturing scenarios involving very limited screw-fastening data. We assume that, over time, entirely new error types will appear, the system has never seen before, and that only very few or none of these unforeseen errors will be obtainable. In a multi-class setting, the FSL models can only recognize new error types if those types appear in the support set. In a multi-label setting, however, the model can detect combinations of known defects even when those exact combinations aren't in the support set. For example, if the support set contains only the uni-factorial defects A and B, a multi-label FSL model can still classify the multi-factorial defect "A, B" without ever having seen that specific combination in the support. In the multi-class setting, FSL applies when new error types are available and screw-fastening multi-labels are converted into distinct classes. If no new error types can be obtained and errors appear only as specific combinations of known defect types, multi-label FSL can be used.

Furthermore, FSL libraries [67, 68] are **label size agnostic**, as these implementations can remap the label when sampling episodes. For instance, if we have one episode with ground truth labels $\{7, 8, 9\}$, the implementations will remap these labels to $\{0, 1, 2\}$ by remapping 7 to 0, 8 to 1 and 9 to 2. This key property ensures no matter how the screw-fastening error types are enriched in the future, the FSL models don't need output dimension change and still fit. Note that these implementations are not working with multi-label dataset. Our adaptions are proposed in section 4.3.

4 Data Preprocessing and Sampling

This chapter details the methodologies employed to preprocess and structure the dataset used in this research. We first present the specific preprocessing steps to refine and format the raw data. Following preprocessing, we describe the approach for data separation and sampling. This includes the strategy for partitioning the dataset into training, validation, and test subsets.

4.1 Data Preprocessing

According to Wolfgang et al. [69], "torque is the most widely used and practically measurable process variable in industrial screw driving processes." Moreover, the predecessors [4, 65] also extracted torque only when preprocessing M6 dataset. Based on these, we focus exclusively on the torque signal. We extract the `torque` column from each sample, reset any invalid values (i.e., torque values less than zero) to zero (the same as Songsik [4]), and apply min-max normalization using the formula:

$$x' = \frac{x - x_{\text{min}}}{x_{\text{max}} - x_{\text{min}}} \tag{4.1}$$

Where:

- x is the original torque value,
- x_{min} is the minimum torque value in the sample,
- x_{max} is the maximum torque value in the sample.

Songsik [4] downsamples each series to 920 points, a target we likewise adopt. Both Songsik [4] and Paulus [65] use a downsampling rate of 20, which we also apply. After downsampling, series exceeding 920 points are truncated. Shorter series are zero-padded to 920 points. Figure 8 illustrates the preprocessing pipeline.

4.2 Data Separation

Following the machine learning common sense [23], the dataset used in this study was systematically divided into three distinct subsets:training, validation, and testing. We ensured that the label distributions in each subset are mutually exclusive in FSL. For instance, label (2,7) and label (1,2) are not mutually exclusive since there's a label overlap on 2. We did the combinatorial assignments over the data labels, trying to place these labels into three slots (training, validation and test) and ensuring no label overlapping. However, no ideal solution exist. Because there're compound labels (357), (267), (16) and (24), it implies any labels involving 1,2,3,4,5,6 and 7 must be placed in one set otherwise it would break the non-overlapping rule. For instance, if we place (24) in one set, then any label involving 2 and 4 should be placed in the set. Since 2 is included, any label involving 2 should be included, for example (267). The logic propagates. ⋯ Eventually, everything except 0 must be be one set. If we allow some labels to be abandoned, there exists a satisfiable solution, as shown in Table 4. Specifically, classes such as (2,7) and (2,6,7) are excluded. For sample count in training, validation and

test set, we keep its ratio to 50:25:25. Normally, it's suggested to be 75:15:15 by mainstream. If we force it to be 75:15:15, we could remove some labels in validation and test set. However, if we remove one label from Table 4, there would be such two cases in validation/test set:

- One multi-label and one single-label in validation/test set
- Two single-labels left in validation/test set

For instance, for validation set, if we remove (24) and leave 2 and 4, we lose the valuable multi-label samples which are the key in our study. If we remove 2 and keep 4 and (24), in multi-label setting (assuming the network outputs by sigmoid), we would lose the opportunity classifying 4 since its ground truth on label 4 is always on. And the same applies when removing label 4. Moreover, removing more than one labels doesn't introduce any meaningful setting since it leads feasible N-way to be 1. Therefore, our proposed solution (Table 4) is acceptable.

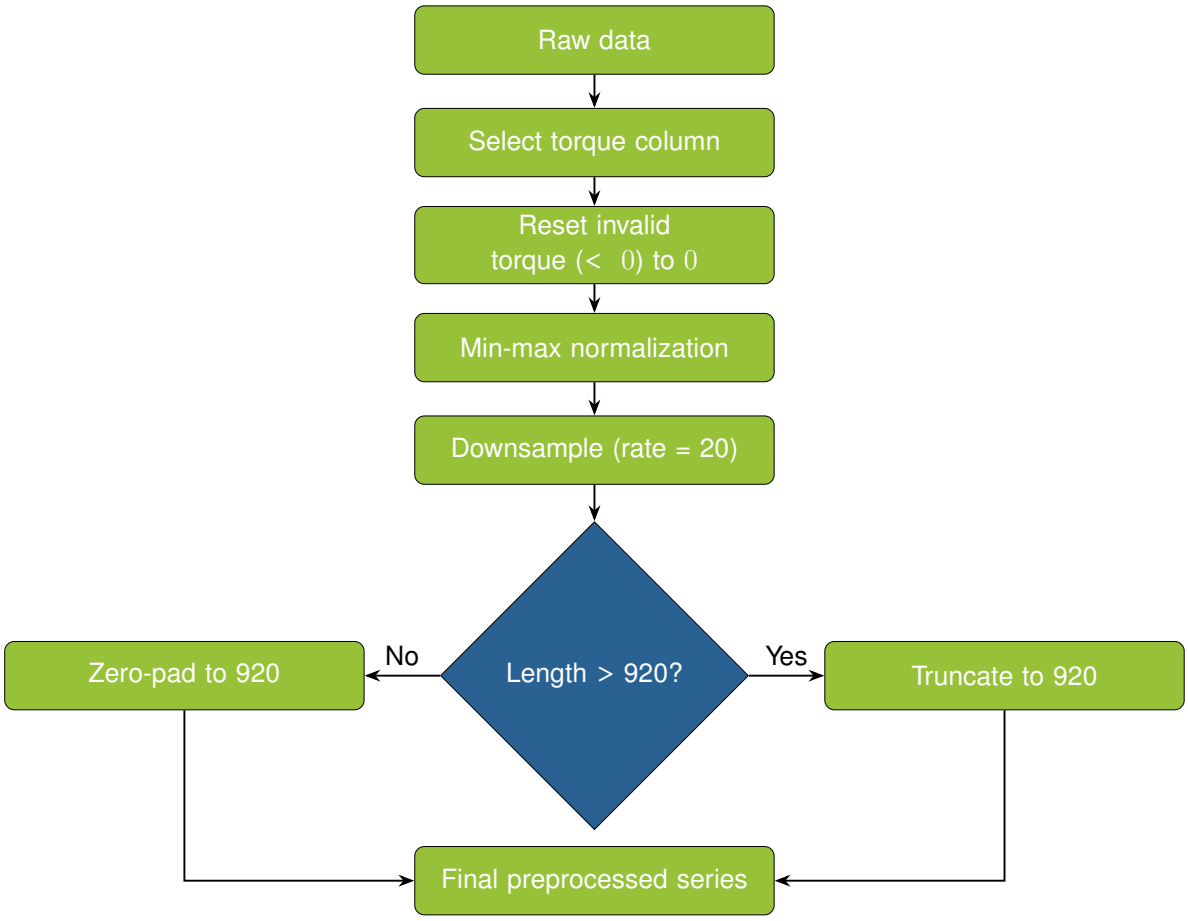

Figure 8: Simplified flowchart of preprocessing screw-fastening raw data

4.3 Episodic Sampling

Our data is multi-labeled and existing FSL episodic sampling is based on multi-class. Therefore, we adapt the multi-label to multi-class. One simplest solution would be assigning every combinational label a unique class ID [70]. We consider the multi-label (represented as binary vectors) as bits, and its integer representation is its unique class ID. Formally, given a

multi-label binary vector $V = (v_1, \cdots, v_n) \in \{0, 1\}^N$, its unique class ID c is:

$$c = \sum_{i=1}^{N} 2^{i-1} \cdot v_i \tag{4.2}$$

The multi-class episodic sampling is always cooperated with multi-class few-shot classification. It might not work well with multi-label few-shot classification. The reason is that it can cause nondeterministic output dimensions, especially when the network relies on a sigmoid layer for multi-label classification. For instance, suppose we have three labels (0,1,2) in our dataset and use N-way=2, unique labels in the first episode can be $\{0, (1, 2)\}$, and unique labels in the second episode can be $\{0, 1\}$.

The output dimensions of first episode should be 3 since there are 3 different labels, and the output dimensions of the second episode is supposed to be 2. we could solve this using the full label representation, always outputting number of labels in the network. However, it loses the flexibility, when the screw-fastening label dimensions changes (e.g. adding a new error type), the model need retraining in this case.

To make network (using sigmoid for final output) flexible for multi-label, we propose a label-based episode sampling. It's based on the idea that multi-label can be thought as several multi-classes simultaneously. For instance, a sample labeled 357 will collapsed into three copies labeled 3, labeled 5 and labeled 7, respectively. For episode sampling, we begin by collapsing all the multi-labels into multi-classes. Afterwards N-way single-labels are selected. Then support set and query set are selected in the same as multi-class episode sampling (chapter 2.1.2). Note that the ground truth labels are not simply remapped when generating support set and query set but adapted in some way. Adaption removes unsampled labels and remaps the labels eventually. For instance, if the sampled labels are $\{1, 3, 7\}$ and three samples selected in support set has ground truth labels $\{(1), (1, 3, 9), (1, 2)\}$, before remapping, the three labels will be transformed to $\{(1), (1, 3), (1)\}$. This multi-label episode sampling ensures the network output dimension is N-way. However, in this way, duplicate samples could appear in the support set sometimes.

Table 4: Data separation overview

Data	Data Labels	Label Count	Sample Count
train	0, 5, 3, 7, (35), (37), (357)	6	1100
validation	2, 4, (24)	3	500
test	1, 6, (16)	3	500
abandoned	(27), (267)	2	200

5 Model Design

This chapter outlines the methodologies employed in the design of the FSL models utilized in this project. First, the Prototypical network [16] approach is discussed. Subsequently, MAML [1] approach is presented. Finally, the backbone architectures are described in detail.

Figure 9 shows the one episode (support set and query set) is inputted into multi-label/multi-class MAML/Prototypical network. Before episode is fed to Multi-class and Multi-class Prototypical network, all multi-labels in episodes are converted to integers (Formula 4.2). Before episode is fed to Multi-label Prototypical network, the activated label space will be calculated, which will be described afterwards. Both multi-label and multi-class MAML need adapting support set and updating gradient. Both multi-class and multi-label Prototypical network require centroid computation. MAMLs reply on logits when classifying query set and Prototypical networks depend on logits on negative distance between query and each centroid. The networks can use logits to update or backpropagate.

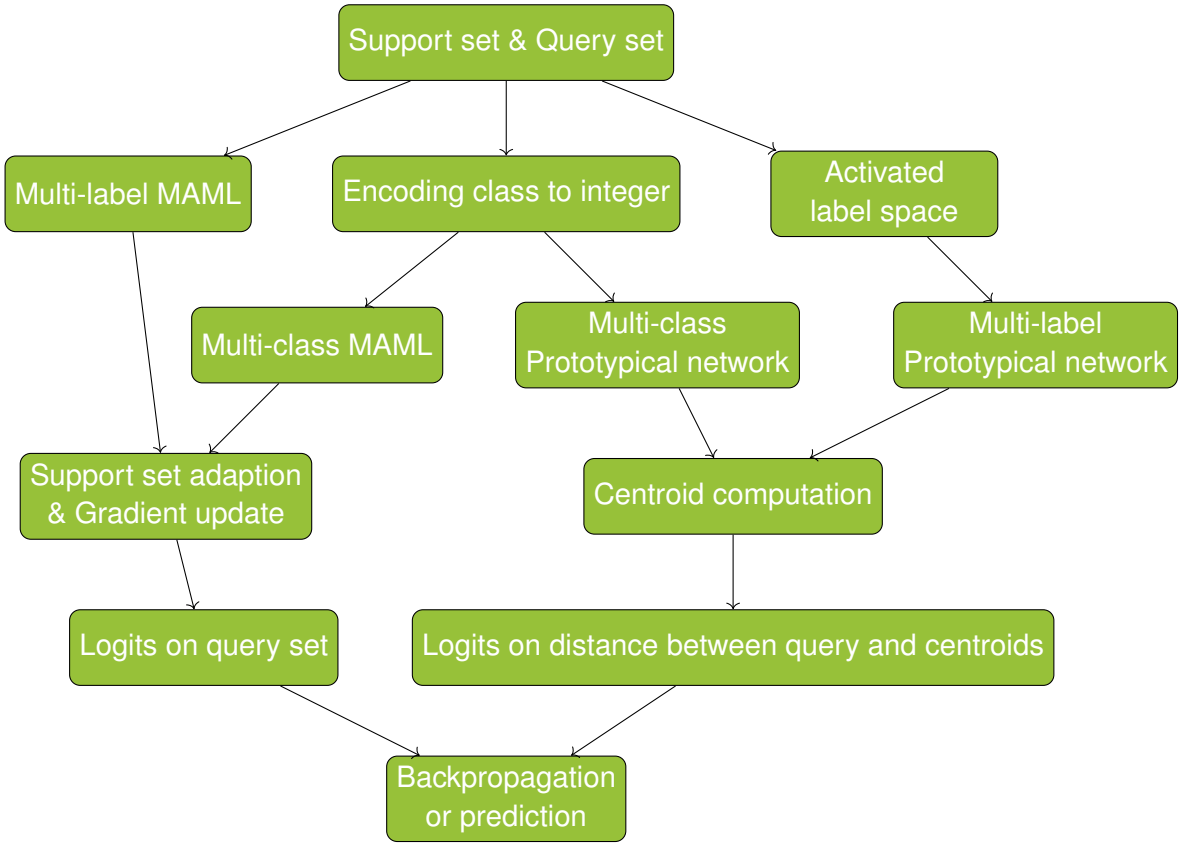

Figure 9: Few-Shot learning methodology pipeline overview. Every node is a procedure except the Support Set & Query set.

5.1 Prototypical Network Approach

5.1.1 Prototypical Network Approach for Multi-Class Setting

We encode our multi-label data into multi-class using Formula 4.2. In this case, every label y_j will be an integer.

Multi-Class Centroid Computation For multi-class, we use the same way to compute centroids from Snell et al. [16]. In each training episode τ_i, data is provided as a tuple consisting of a support set S_{τ_i} and a query set Q_{τ_i}. Initially, the samples within the support set are fed into the network backbone f to obtain their respective embeddings. Utilizing the provided labels, we compute the prototypes C_l by averaging the embeddings corresponding to each class l as [16]:

$$C_l = \frac{1}{N_l} \sum_{(x,y) \in S_{\tau_i}} f(x;\theta) \text{ if } y = l \tag{5.1}$$

where N_l is number of samples whose label = l in S_{τ_i}.

Query Set Prediction & Loss Function Subsequently, the query set passes through the backbone to generate embeddings. We then measure the distance between each query embedding and each class prototype. The negative distance to each centroid will be fed into Softmax to make logits. Finally, the cross-entropy loss between logits and true labels is computed as [16]:

$$\mathcal{L}(\theta) = \frac{1}{|Q_{\tau_i}|} \sum_{(x,y) \in Q_{\tau_i}} L_{ce}(logits, y) \tag{5.2}$$

where

$$logit = Softmax(-d(f(x;\theta), C)) \tag{5.3}$$

d is the distance function (e.g. Euclidean distance) and C is the collection where each entry is a class centroid.

5.1.2 Prototypical Network Approach for Multi-Label Setting

For scenarios involving multiple labels, we change the way of computing centroids and adapt the LC-Protonets [43] framework.

Activated Label Space For a sample labeled as (A,B), it exhibits the characteristics of class A, class B and class (AB). Therefore, we say label (A,B) has the label space $\{A, B, (A, B)\}$. The label space of a multi-label is the power set [71] of each individual component, excluding the empty set [43].

For each episode τ_i with a support set S_{τ_i} and a query set Q_{τ_i}, we first compute the activated

label space A_i, excluding the empty set:

$$A_i = \bigcup_{(x,y)\in S_{\tau_i}} \mathcal{P}(supp(y)) \setminus \varnothing \tag{5.4}$$

where

$$supp([l_1, l_2, \ldots, l_m]) = \{i \mid l_i \neq 0\} \tag{5.5}$$

$supp$ denotes activated labels, $\mathcal{P}$ denotes power set [71], and y is a multi-label binary vector.

Multi-Label Centroid Computation We apply the same methodology from LC-protonet [43] to compute centriods. For a label $l \in A_i$, to compute its centroid C_l, samples contribute to the centroid as long as their labels include l [43]. For instance, one sample labeled as (A, B) contributes to class A's centroid. For a label $l \in A_i$, its centroid is computed as follows:

$$C_l = \frac{1}{N_l} \sum_{(x,y)\in S_{\tau_i}} f(x;\theta) \text{ if } l \in \mathcal{P}(supp(y)) \tag{5.6}$$

where N_l is the number of samples whose label is covered by l.

After computing the centroids, we process the query set in a manner similar to the standard Prototypical network used for multi-class classification. We compare the distance between the query samples and centroids and make predictions based on this. However, since we are dealing with multi-label classification, we decode the prediction into multi-label with the help of label space A_i. The complete pipeline is illustrated in Figure 10.

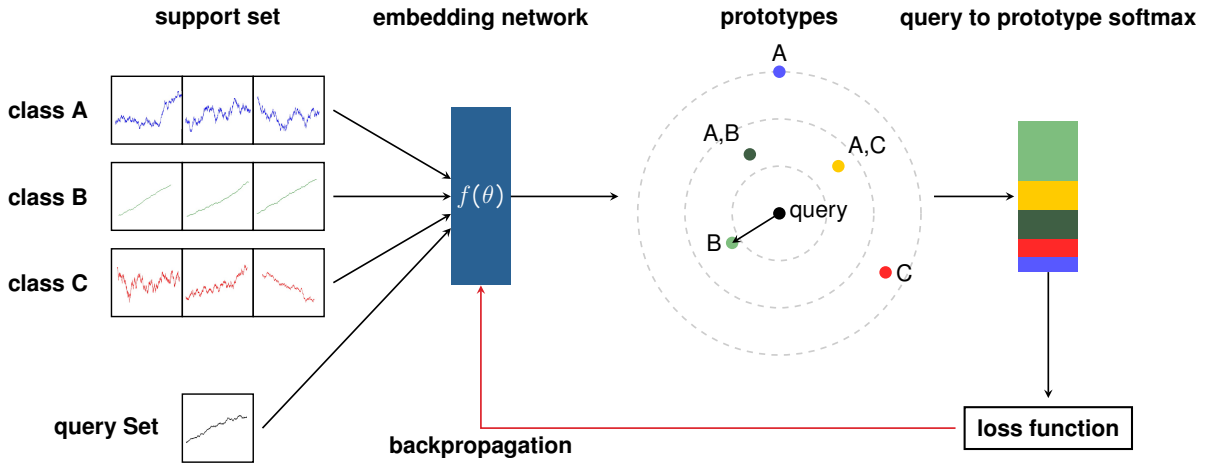

Figure 10: The Prototypical Network pipeline for multi-label screw-fastening data, where there are centroids for the activated labels in the representation space. Here, we apply softmax on negative distance from query to each prototype. For simplicity, here we use real label instead of one-hot encoding representation.

5.2 Model Agnostic Meta-Learning Approach

We begin with a single model called the meta-model, denoted by Θ. For each training episode τ_i, consisting of a support set S_{τ_i} and a query set Q_{τ_i}, we create a cloned instance of the meta-model, which we refer to as the learning model, denoted by θ.

Support Set Adaption & Learning Model Update During each episode, the support set is fed through the learning model, which includes a backbone and additional dense layers. The dense layer output then passes through an activation function—typically softmax for multi-class classification or sigmoid for multi-label settings. A loss is computed using the cross-entropy loss function. This loss is used to update the learning model parameters θ via a gradient descent step [1]:

$$\theta_i = \Theta - \sum_{(x,y)\in S_{\tau_i}} \alpha \nabla_{\Theta} L(f(x;\Theta), y) \tag{5.7}$$

where L is the cross entropy loss and α is the learning rate.

Query Set Adaption & Meta Model Update Next, the query set Q_{τ_i} is fed into the updated learning model θ_i, and we check the output f_{θ_i} and compute the loss. This loss is then back-propagated through the learning model to update the meta-model Θ. Since the learning model is derived from the meta-model, this process introduces second-order gradients (i.e., Hessian gradient) w.r.t Θ [1]. In episode τ_i, the meta-model is updated using [1]:

$$\Theta = \Theta - \beta \nabla_{\Theta} \sum_{(x,y)\in Q_{\tau_i}} L(f(x;\theta_i), y) \tag{5.8}$$

where β is the learning rate for meta model.

Figure 11 provides an overview diagram containing steps in MAML during one training episode.

Furthermore, during learning model adaptation, we allow it to adapt multiple times for one episode. Algorithm 1 shows the pseudo-code of how we train MAML within the episode.

During inference, the model still follows the similar pipeline. The learning model still be copied from the meta model. It will still adapts the support set. However, when it finishes adaption, it will classify the query set.

5.3 Backbone

The following section introduces the backbones we used in this project and discusses what we adapted for them. The encoders we used are 1D-CNN, InceptionTime, and Moment.

5.3.1 1D CNN

Our 1D-CNN encoder adopts a standard architecture [34] consisting of N convolutional blocks followed by M dense blocks. Each convolutional block includes a convolutional layer, a pooling layer, batch normalization, and dropout. The output from the final convolutional block is

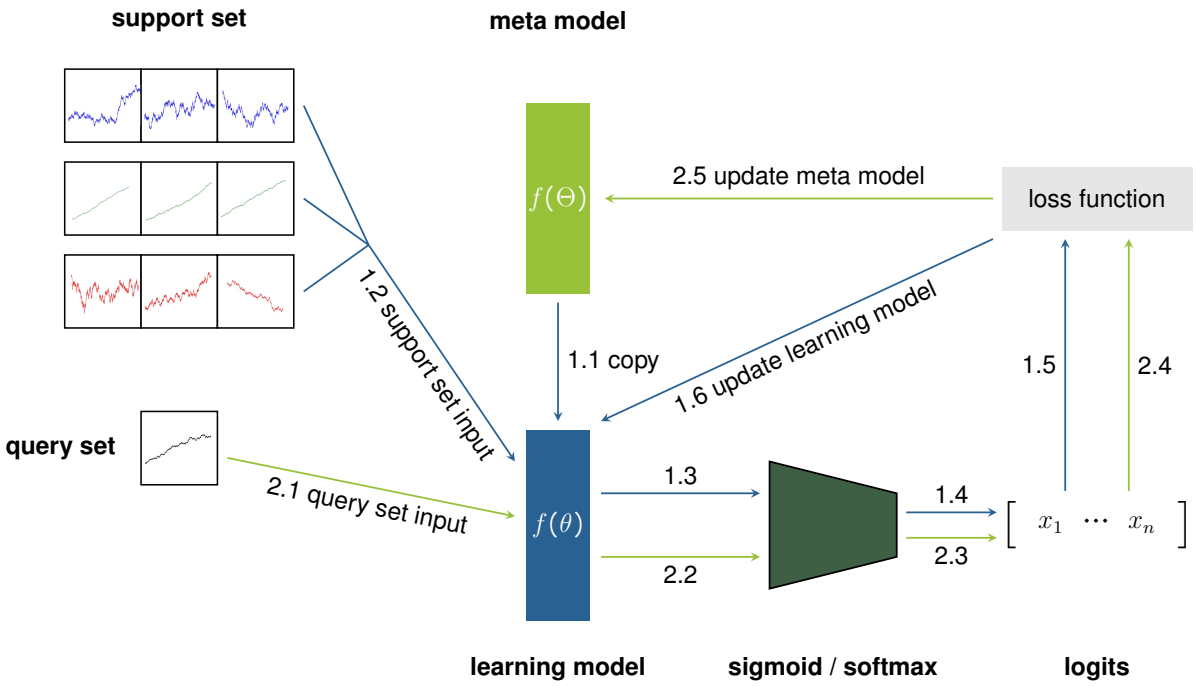

Figure 11: MAML training pipeline overview. In one episode, the learning model is first initialized from meta model. Then support set is fed to the learning model. The loss generated from this is backpropagated to learning model itself. Afterwards the query set is fed to learning model, the loss generated is backpropgated to meta model. 1.X indicates the steps during support set adaption. 2.X denotes the steps handling query set.

Algorithm 1 MAML training procedure (adapted from [1])

Require: adaption step M, initial parameter Θ
Require: Training Episodes 1...N.
Require: support set S_{τ_i} and query set Q_{τ_i} for each episode τ_i
Require: α and β: learning rate and meta-learning rate

for $i = 1$ to N **do** ▷ For each training episode
  $\theta_i = \Theta$
  for $z = 1$ to M **do** ▷ Adapt support set for M times
    $\mathcal{L} = \sum_{(x,y)\in S_{\tau_i}} L(f(x;\theta_i), y)$ ▷ Loss on support set
    $\theta_i = \theta_i - \alpha\nabla_{\theta_i}\mathcal{L}$ ▷ Learning model updates
  end for
  $\mathcal{L} = \sum_{(x,y)\in Q_{\tau_i}} L(f(x;\theta_i), y)$ ▷ Performance on query set and gather loss
  $\Theta = \Theta - \beta\nabla_{\Theta}\mathcal{L}$ ▷ update meta model
end for

flattened and passed through the dense blocks composed of fully connected layers. The output of the last dense layer is then fed into a final linear layer that projects it to the desired representation dimension. Figure 12 illustrates the overall architecture.

5.3.2 InceptionTime

We do not introduce significant modifications to the original InceptionTime architecture [2]. In our implementation, the network comprises d sequences Inception modules. For each Inception module, we set the three kernel sizes to 39, 19, and 9, respectively. This differs from the original configuration proposed in Fawaz et al. [2], which used even-sized kernels such as 40. Our choice to use odd kernel sizes was made to preserve symmetry in convolution operations [72]. The detailed structure of an Inception module is illustrated in Figure 13. Following the Inception modules, the output is passed through dense layers, which follows the same configuration depicted in Figure 12.

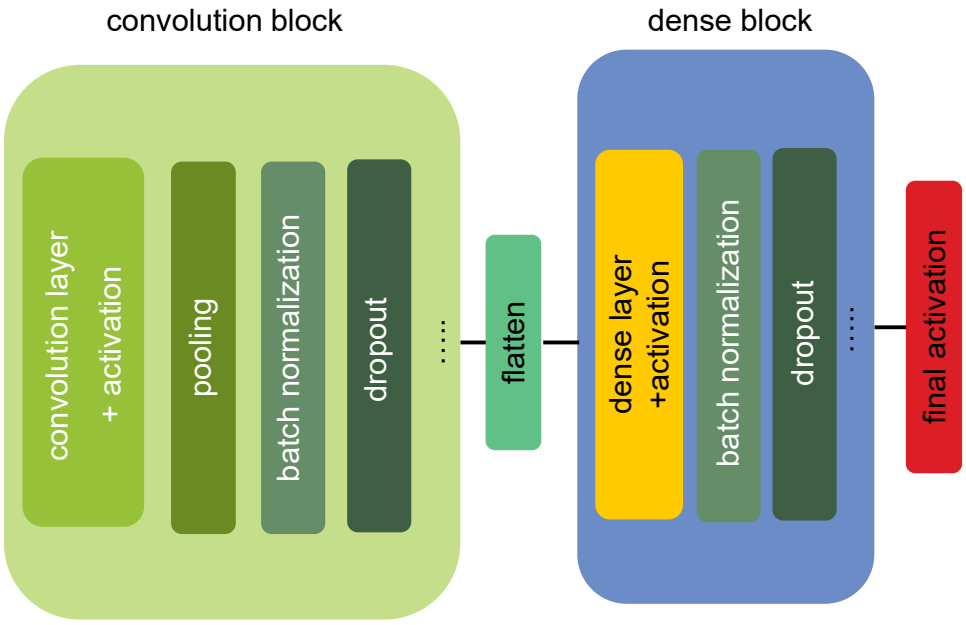

Figure 12: 1D CNN architecture used in this project

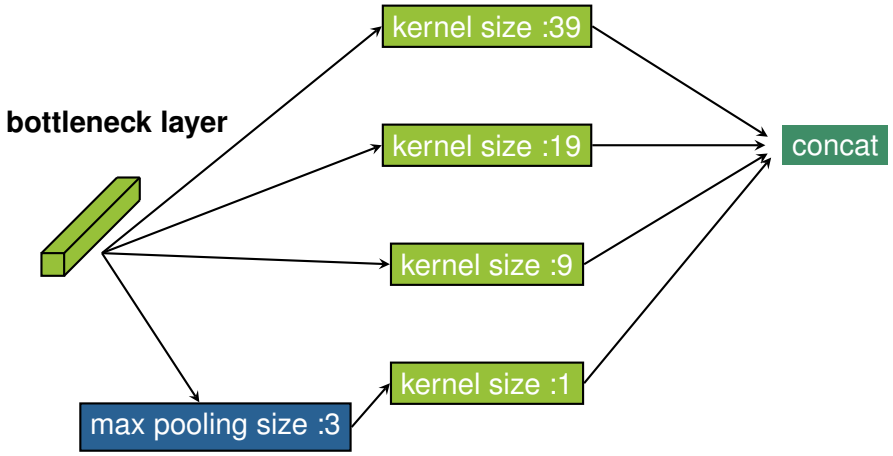

Figure 13: Inception module used in this project.

5.3.3 Moment

The Moment has several variants, Moment Small, Moment Base and Moment Large. We use Moment Large given that it has highest performance in open public benchmarks [3]. Moment Large contains approximately 341M parameters and consists of 24 T5 encoder blocks [3]. A T5 encoder block [5] is a variation of transformer encoder [73]. In Moment Large, one T5 encoder block uses d_model of dimension 1024 and feedforward layers of dimension 4096, with a 16 attention heads [74]. It means that all the q layers, v layers and k layers are 1024×1024 linear layers. The architecture can be found in Figure 14.

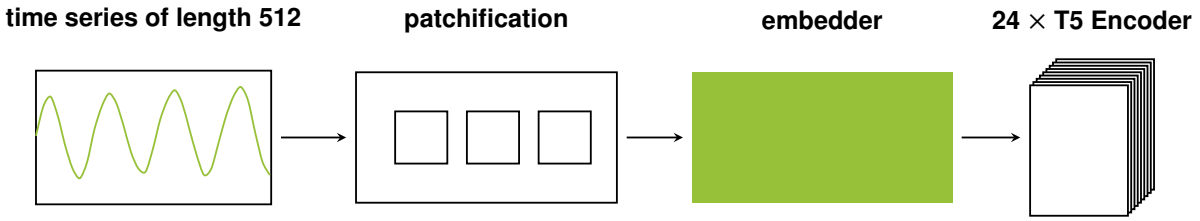

Figure 14: Moment (large) architecture for representation learning [3]. The main architecture consist of patchification, patch embedder and a sequence of T5 Encoder blocks. It takes a 512 lengthed time series and output a representation vector of 1024 dimensions in the end. One T5 encoder [5] is a variant of transformer encoder. The embedder is simply one linear layer that maps from patch diemsnion to 1024.

For Moment, since it's pretrained, we can directly freeze it for faster computation speed and a balanced performance. Another option is finetuning Moment. The option full finetuning is not considered because of its large parameter size and scarcity of data in FSL. The option finetuning the last dense layer might be considered. However, in Moment encoder the structure is not designed with a pretrained final dense layer. It might inspire us to consider finetune the last T5 encoder. Nevertheless, one T5 still contains 3M+ parameters and is still large. Therefore finetuning the last T5 is not planned. A partial finetuning inside the last T5 might be proposed but we didn't find too much work regarding finetuning partially inside one transformer encoder. We only finetune via Low-Rank Adaptation of Large Language Models (Lora) [75]. Lora approximates dense-weight matrices using low-rank decomposition. By multiplying a low-rank vector by its transpose, one matrix can be obtained, which can be further as gradient deviation for a linear layer update [75].

Since the Moment only takes a time series of length 512 [3], we add an additional down-sampling module for prepreprocessed data of length 920. It downsamples at rate of 2 and afterwards pads to 512. Another method to feed our preprocessed data is to truncate, removing any information after time point 512. However, this might reduce the information as some spatial information hides in the latter part. One promising solution is chunking. In this case, we can chunk our 920 lengthed time series into two 512-step chunks. The first chunk is first 512 time step data and, likewise the second chunk take the remaining and is padded to length 512. Feeding these chunks in parallel into Moment will obtain two representation vectors. The first representation vector encodes self attention information of the first chunk. Also the second representation vector encode the second chunk. We might need attention between the first chunk and second chunk, therefore requiring the full representation combining the first and second chunk. However, in order to have the full representation of the whole series, we might need to fuse two representation vectors, which may require apply some networks. Moreover,

we are not sure which architecture to utilize for fusion, and it might bring more computation time. Therefore, by Occam's razor, we decided to discard this.

The Moment used in this report have four variants:

- Frozen Moment. Exactly the same in Figure 14 with all pretrained weights frozen, including embedder and all the T5 encoders.
- Frozen Moment + linear. The frozen Moment is appended with several tunable linear layers.
- Lora Moment. The Moment is finetuned with Lora for all transformer modules in all T5 encoders.
- Lora Moment + linear layer. The Lora Moment is appended with several dense layers.

The dense layer follows the same architecture of that in Figure 12.

5.4 Specification

As mentioned before, FSL methodologies provide framework for FSL pipeline how to adapt the support set and classify the query set. All the FSL methodologies in our project require a backbone to represent the input time series. For different FSL methodologies and backbones, we might need some specifications. In this section, we discuss these FSL methodologies and backbones' specificity.

Prototypical Network For Prototypical network, it's metric-based FSL methodology, therefore, it's dependent on backbone. The whole pipeline keeps the same no matter what backbone is uses. In this report, we equip Prototypical network with 1D CNN, InceptionTime and all Moment variants. When used with frozen Moment, during backbropagation, the gradients will stop on the last layer of the frozen Moment.

MAML Unlike Prototypical network, MAML replies on tunable parts. The backbone must have some tunable sections. Therefore, the frozen Moment can't be adopted by MAML. Moreover, MAML in our project uses second-order gradient (Hessian gradient), requiring the number of parameters to be small for computation speed. If we use Moment Lora and finetune 1% of total parameters, we still have around 4M parameters and memory complexity is $\mathcal{O}(n^2)$ for Hessian gradient. Therefore, we decide our MAML not to use Moment Lora and Moment Lora + linear. The only option left to be backbone is frozen Moment + linear. For lightweight backbones, 1D CNN and InceptionTime, MAML is free to use.

Backbones During training, we allow some hyperparameters (e.g. epoch) determined by backbones. For lightweight backbones, 1D CNN and IncpetionTime, we set it a large one 200. For Moment, we received some inspiration a Moment tutorial [76], where it sets 1 epoch on performing a forecasting task on ETDataset [77]. However, the ETDataset has 30,000 samples, each with 7 features. We didn't find the proportion of training set in the tutorial. We assume the training set of ETDataset is 70%. The number of samples it iterate over 1 epoch is 21,000. Our training set contains 1100 samples. If we iterate all training samples in one epoch, the expected epoch is roughly 20, which we set in the experiments.

6 Experimental Results and Discussion

We conduct experiments for two FSL methodologies, Prototypical network, and MAML, with three types of backbones: 1D CNN, InceptionTime, and Moment. Moreover, we have two ways to sample a few shot learning data: by class or by label. We will conduct experiments using different methodologies, backbones, and data sampling configurations in combination. We follow the regular train-validation-test machine learning pipeline [78]. But instead of finding the best checkpoint, we are more interested in robustness of a model. Therefore, we wish to find the best hyperparameter and evaluate it, as show in Figure 15.

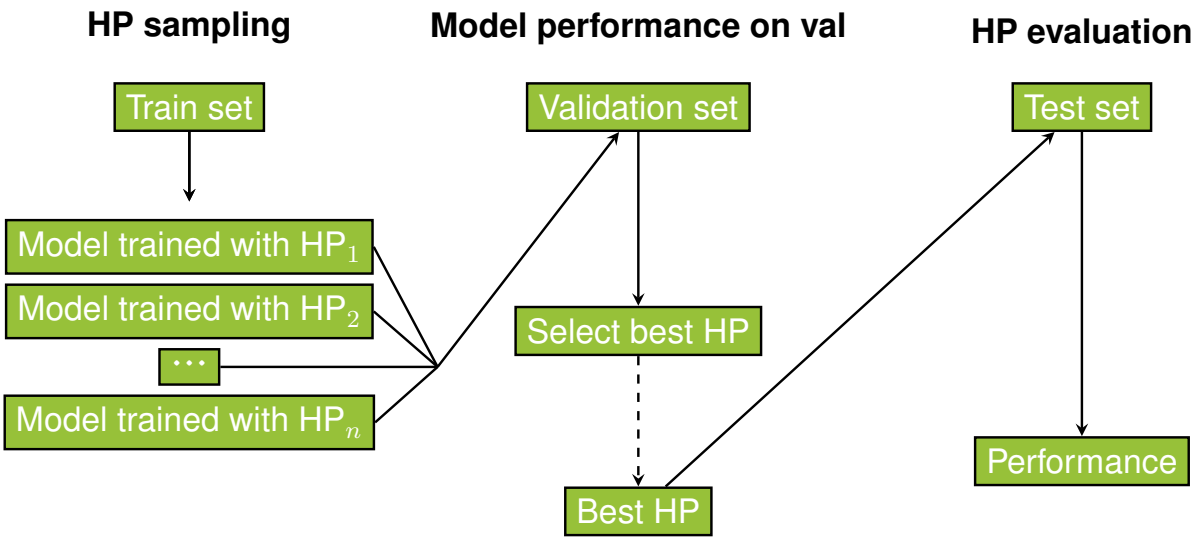

Figure 15: Experiment pipeline. Initially we sample HPs and use this hyperparameter to obtain a trained model. The trained model is then recorded regarding its performance on validation set. In the end, the best HP leading to best performance on validation set is selected. The it comes to test evaluation. The best HP initalize final model. The final model is trained on training set and evaluated on test set. It performance on test set will be recorded. This test evaluation is conducted for several times. The hyperparameter sampling method is the Bayesian based sampling method from Optuna [6]. Abbreviations in this figure: HP (Hyperparameter).

6.1 Hyperparameter Setting

This section discusses the hyperparameters that each model and methodology owns. It provides details regarding the hyperparameter's meaning and range.

6.1.1 Basic Hyperparameter

Every FSL methodology has a hyperparameter for the learning rate, weight decay, optimizer and early stop patience. Its detail can be found in Table 5.

Table 5: Basic Hyperparameter. If the a hyperparameter is fixed, it's not considered for hyperparameter optimization.

Hyperparameter	Range
learning rate	$[10^{-6}, 10^{-4}]$
weight decay	$[10^{-6}, 10^{-4}]$
optimizer	{Adam, SGD, AdamW, RMSprop}
patience	5

6.1.2 MAML Hyperparameter

For different methodologies, we have different specific hyperparameters. For MAML, we have two hyperparameters, meta-learning rate, and adaption steps. Meta-learning rate species the rating rate for gradient update for meta-model. Adaption steps control how many iterations the learning model learns the support set. Table 6 shows the hyperparameter range.

6.1.3 Prototypical network Hyperparameter

We have two hyperparameters for the Prototypical network: normalization and distance function. Normalization is a boolean choice whether we apply L2-normalization or not. We use The distance function to calculate the distance between two representation vectors. Table 6 shows the hyperparameter range.

Table 6: Hyperparameters and their ranges for different FSL methodologies.

FSL Methodology	Hyperparameter	Range
MAML	meta-learning rate	$[10^{-6}, 10^{-4}]$
	adaption step	[5, 15]
Prototypical network	normalization	{True, False}
	distance	{Cosine, Euclidean}

6.1.4 Backbone-Specific Hyperparameter

For 1D CNN, several critical hyperparameters are the number of convolutional layers, number of channels, kernel size, pooling function, pooling kernel size, and convolution activation function. For InceptionTime, the number of inception modules, the number of filters, and the output dimension are critical hyperparameters. For Moment, if it is not frozen, we have Lora rank, Lora alpha, and target module as hyperparameters. Since Moment is a pretrained foundation model, we use a tiny epoch, 20. For other lightweight backbones, we fix the epoch to 200. Table 7 shows the each hyperparameter details. The full hyperparameters for each backbone can be found in Appendix A.

Table 7: Backbone-Specific critical hyperparameters. The epoch is fixed for all backbones and not taken account in optimization.

Backbone	Critical Hyperparameters	Range
1D-CNN	number of conv layer	[2, 6]
	kernel size each conv	[3, 11]
	number of channel each conv	[16, 64]
	pooling	{Max, Avg}
	pooling kernel Size	[2, 4]
	conv activation function	{Relu, Selu, Elu, mish}
	epoch	200
Moment (Lora)	Lora rank	[2, 8]
	Lora alpha	[2, 16]
	target module	{{q}, {v}, {q,v}}
	epoch	20
InceptionTime	number of Inception modules	[2, 5]
	number of filters	[4, 16]
	representation dimension	[64, 125]
	epoch	200

6.2 Experiment Setting

Our experiments are conducted on a machine running Debian GNU/Linux 12.0. The system is equipped with an NVIDIA GeForce RTX 2080 GPU featuring 8 GB of VRAM, which is sufficient for FSL data scarity cases. All code is written in Python 3.10 and executed with CUDA 11.8 to enable GPU acceleration. To realize episodic sampling, we make use of the Learn2Learn library [67].

To simulate scarcity of data, we set K-shot=10. If we use class-based sampling (Chapter 4.3) with labels encoded into multi-class, we set N-way=3. If we use label-based sampling (Chapter 4.3), since we only have two distinct labels in validation set and test set, for the maximum N-way, we can only set it 2. Since the number of samples for every categories ≥ 100, deducting the K-shot for the support set, the would remain at least 90 samples for each category. we could set M-query=90, but considering of possibility of potential bugs in the code, we set M-query=50, a stable number instead. For the number of episodes, we set number of episodes in training to 60, number of episodes in validation to 30 for faster computation and number of episodes in test to 100 for accurate results.

6.3 Experiment Results

We use optuna [6] to find the best hyperparameter found from validation set and trained on training set. We use multiple objectives in Optuna, precision, recall and F1 score. The best hyparameter is selected by F1 score. With the best hyperparameter, we conduct training multiple times and record its performance on the test set. For lightweight models, i.e., 1D CNN and InceptionTime, we conduct it up to 50 times. For Moment, we only conducted training 15 times due to its large number of parameters which takes long. The evaluation results can be found in Table 8, using the weighted F1 score, considering the class imbalance.

Moreover, for each model, we find its best methodology, as shown in Table 9. Furthermore we calculated metrics for each class metrics the best (model,methodology) behaves in the test set, as shown in Table 10.

In terms of time, hyperparameter search of 100 trials and evaluation experiments on lightweight models can be taken within one day. However, for Moment, it takes longer. The hyperparameter search on Moment Lora (without/with linear) for 100 trials takes around four days. Moreover, its evaluation can be finished within two days. For frozen Moment (without/with linear), the hyperparameter search can be finished within two day. The evaluation can be done within one day.

6.4 Summary and Discussion of Experimental Results

Based on the evaluation results in Table 8 and the class-wise performance comparison in Table 10, we have observed that InceptionTime consistently achieves the highest weighted F1 scores in both multi-class and multi-label settings under the Prototypical network methodology. Specifically, it achieves an F1 score of 0.944 in multi-class and 0.935 in multi-label classification. While Moment is expected to perform best, in most cases, it fail to underperform 1D CNN. Extra downsampling for Moment (mention in Chapter 5.3.3) can be the reason. Another reason can be our insufficient data. From a use case [76], where they finetune Moment on ET-Dataset [77] consisting of around 30,000 samples with 7 features for one epoch. Though, we have only have 1100 samples in our training set, for which we increase the epoch to 20. This might lead to overfitting. Furthermore, the frozen Moment encoder (direct evaluation) shows the lowest performance. However, applying Lora adaptation and adding a linear classifier significantly improves Moment's performance.

Across all backbones, the Prototypical network generally outperforms MAML. For example, InceptionTime achieves 0.944 under the Prototypical network compared to 0.912 under MAML. This hits our impression that Prototypical network generally outperforms MAML, as the open benchmark [79] shows the same tendency.

From Table 10, InceptionTime and 1D CNN provide a balanced trade-off between precision and recall. While the fine-tuned Moment model achieves the highest precision for individual classes, its relatively lower recall results in a slightly reduced F1 score. InceptionTime offers the best overall balance, maintaining high scores across all metrics and class groupings.

InceptionTime with Prototypical network emerges as the most effective and robust combination for FSL. It outperforms the extensive pretrained backbones.

Table 8: Model F1 Scores across FSL methodologies. The best hyperparameter is chosen to evaluate on the test set. The lightweight models are evaluated 50 times. For Moment, we evaluated it 15 times. The evaluation uses sklearn [7] weighted F1 score. The model with the highest mean in each methodology is marked bold. The F1 column is in the format mean ± standard deviation.

Methodology	Backbone	F1
multi-class Prototypical network	Moment (directly eval, frozen)	0.818 ± 0.002
	Moment Lora	0.864 ± 0.008
	Moment (frozen + linear)	0.879 ± 0.008
	Moment (Lora + linear)	0.896 ± 0.005
	1D CNN	0.918 ± 0.01
	InceptionTime	**0.944 ± 0.017**
multi-label Prototypical network	Moment (directly eval, frozen)	0.884 ± 0.002
	Moment Lora	0.9275 ± 0.013
	Moment (frozen + linear)	0.9229 ± 0.008
	Moment (Lora + linear)	0.9312 ± 0.009
	1D CNN	0.9334 ± 0.011
	InceptionTime	**0.935 ± 0.017**
multi-class MAML	**1D CNN**	**0.924 ± 0.005**
	InceptionTime	0.912 ± 0.08
	Moment (frozen + linear)	0.882 ± 0.08
multi-label MAML	**1D CNN**	**0.9169 ± 0.004**
	InceptionTime	0.8944 ± 0.002
	Moment (frozen + linear)	0.8970 ± 0.0019

Table 9: The best FSL methodology for each backbone, where we select by mean of weighted F1 score on test set and Moment denote the Lora Moment + linear.

Backbone	Best FSL Methodology	F1
1D CNN	multi-label Prototypical network	0.9334 ± 0.011
InceptionTime	multi-label Prototypical network	0.935 ± 0.017
Moment	multi-label Prototypical network	0.9312 ± 0.009

Table 10: Performance comparison across different classifiers and classes in the test set measured in weighted precision, weighted recall and weighted F1.The F1 column is in the format mean ± standard deviation.

Data class	Best 1D CNN			Best InceptionTime			Best Moment (Lora + linear)		
	precision	recall	F1	precision	recall	F1	precision	recall	F1
class 1	0.96 ± 0.01	0.90 ± 0.02	0.93 ± 0.01	0.96 ± 0.02	0.93 ± 0.02	0.94 ± 0.01	0.99 ± 0.02	0.88 ± 0.03	0.94 ± 0.01
class 6	0.94 ± 0.01	0.93 ± 0.02	0.93 ± 0.01	0.95 ± 0.03	0.94 ± 0.01	0.95 ± 0.01	0.98 ± 0.03	0.89 ± 0.01	0.93 ± 0.01
class 1,6	0.94 ± 0.01	0.90 ± 0.03	0.92 ± 0.02	0.96 ± 0.05	0.93 ± 0.03	0.94 ± 0.03	0.96 ± 0.05	0.88 ± 0.03	0.91 ± 0.03

7 Conclusion and Outlook

7.1 Conclusion

This study investigated the applicability of FSL techniques—namely Prototypical network and MAML for time series classification in industrial screw-fastening scenarios. We explored multiple backbone architectures, including 1D CNN, InceptionTime, and Moment, and evaluated their performance under multi-class based and multi-label based episode sampling.

The results show that lightweight models such as 1D CNN and InceptionTime outperform foundation models like Moment, espeically when leveraged with Prototypical network in multi-class and MAML. However, when leveraging advanced finetuning techniques such as Lora and additional dense layers, the Moment model showed competitive performance, with approximate increase of 7% in weighted F1 score. These findings underline the trade-off between model complexity, computational resources, and classification performance in few-shot scenarios.

Despite the challenges of limited labeled data, our experiments demonstrate that carefully tuned FSL models can perform highly on screw-fastening dataset. The class-based and label-based episode training strategy contributed significantly to this success.

7.2 Outlook

Several directions remain for extending and improving the current work. Increasing the number of classes in training and evaluation tasks may lead to more comprehensive benchmark and improved model generalization.

Second, future research may explore alternative FSL, particularly memory-augmented models. Architectures such as Memory-Augmented Relation Networks [80] are designed to incorporate external memory modules, which could enable more effective handling of sparse or novel instances by enhancing the model's benchmarks.

Additionally, expanding the range of parameter-efficient fine-tuning methods for large foundation models holds promise. Techniques such as Adapter [81] offer may improve performance. When applied to time series classification tasks, these methods could complement or surpass current approaches like Lora. Furthermore, applying a state-of-art FSL episode sampling is recommended. One method [55] sampling the episode from easy to hard could make the learning stage more snooze.

Finally, applying first-order variants of MAML could be a practical alternative to the standard second-order formulation. By significantly reducing memory and computational demands during training, first-order MAML would enable scalable integration of meta learning with a large foundation model.

Bibliography

[1] C. Finn, P. Abbeel, and S. Levine, “Model-agnostic meta-learning for fast adaptation of deep networks,” in *Proceedings of the 34th International Conference on Machine Learning - Volume 70*, ser. ICML’17. JMLR.org, 2017, p. 1126–1135.

[2] H. Ismail Fawaz, B. Lucas, G. Forestier, C. Pelletier, D. F. Schmidt, J. Weber, G. I. Webb, L. Idoumghar, P.-A. Muller, and F. Petitjean, “Inceptiontime: Finding alexnet for time series classification,” *Data Mining and Knowledge Discovery*, vol. 34, no. 6, p. 1936–1962, Sep. 2020. [Online]. Available: http://dx.doi.org/10.1007/s10618-020-00710-y

[3] M. Goswami, K. Szafer, A. Choudhry, Y. Cai, S. Li, and A. Dubrawski, “Moment: A family of open time-series foundation models,” in *International Conference on Machine Learning*, 2024.

[4] S. Songsik, “Erprobung unterschiedlicher maschineller lernverfahren zur schraubprozessüberwachung bei einzelnen und kombinierten fehlerfällen am beispiel der elektromotorenendmontage,” Master thesis, Friedrich-Alexander-Universität Erlangen-Nürnberg, Erlangen, Germany, 2023.

[5] C. Raffel, N. Shazeer, A. Roberts, K. Lee, S. Narang, M. Matena, Y. Zhou, W. Li, and P. J. Liu, “Exploring the limits of transfer learning with a unified text-to-text transformer,” *Journal of machine learning research*, vol. 21, no. 140, pp. 1–67, 2020.

[6] T. Akiba, S. Sano, T. Yanase, T. Ohta, and M. Koyama, “Optuna: A next-generation hyperparameter optimization framework,” in *Proceedings of the 25th ACM SIGKDD International Conference on Knowledge Discovery & Data Mining*, ser. KDD ’19. New York, NY, USA: Association for Computing Machinery, 2019, p. 2623–2631. [Online]. Available: https://doi.org/10.1145/3292500.3330701

[7] F. Pedregosa, G. Varoquaux, A. Gramfort, V. Michel, B. Thirion, O. Grisel, M. Blondel, P. Prettenhofer, R. Weiss, V. Dubourg, J. Vanderplas, A. Passos, D. Cournapeau, M. Brucher, M. Perrot, and E. Duchesnay, “Scikit-learn: Machine learning in python,” *J. Mach. Learn. Res.*, vol. 12, no. null, p. 2825–2830, Nov. 2011.

[8] Y. LeCun, Y. Bengio, and G. Hinton, “Deep learning,” *nature*, vol. 521, no. 7553, p. 436, 2015.

[9] D. Karimi, H. Dou, S. K. Warfield, and A. Gholipour, “Deep learning with noisy labels: Exploring techniques and remedies in medical image analysis,” *Medical Image Analysis*, vol. 65, p. 101759, 2020. [Online]. Available: https://www.sciencedirect.com/science/article/pii/S1361841520301237

[10] Y. Wang, Q. Yao, J. T. Kwok, and L. M. Ni, “Generalizing from a few examples: A survey on few-shot learning,” *ACM Comput. Surv.*, vol. 53, no. 3, Jun. 2020. [Online]. Available: https://doi.org/10.1145/3386252

[11] S. Chen, Y. Zheng, D. Lin, P. Cai, Y. Xiao, and S. Wang, “Maml-kalmannet: A neural network-assisted kalman filter based on model-agnostic meta-learning,” *IEEE Transactions on Signal Processing*, 2025.

[12] M. Abbas, Q. Xiao, L. Chen, P.-Y. Chen, and T. Chen, “Sharp-maml: Sharpness-aware model-agnostic meta learning,” in *International conference on machine learning*. PMLR, 2022, pp. 10–32.

[13] B. Sun, K. Gong, W. Li, and X. Song, “Metar: Few-shot named entity recognition with meta-learning and relation network,” *IEEE Transactions on Audio, Speech and Language Processing*, 2025.

[14] J. J. Valero-Mas, A. J. Gallego, and J. R. Rico-Juan, “An overview of ensemble and feature learning in few-shot image classification using siamese networks,” *Multimedia Tools and Applications*, vol. 83, no. 7, pp. 19 929–19 952, 2024.

[15] J. Luo, H. Shao, J. Lin, and B. Liu, “Meta-learning with elastic prototypical network for fault transfer diagnosis of bearings under unstable speeds,” *Reliability Engineering & System Safety*, vol. 245, p. 110001, 2024.

[16] J. Snell, K. Swersky, and R. Zemel, “Prototypical networks for few-shot learning,” in *Proceedings of the 31st International Conference on Neural Information Processing Systems*, ser. NIPS’17. Red Hook, NY, USA: Curran Associates Inc., 2017, p. 4080–4090.

[17] G. Koch, R. Zemel, and R. Salakhutdinov, “Siamese neural networks for one-shot image recognition,” in *Proceedings of the 32nd International Conference on Machine Learning (ICML) Deep Learning Workshop*, 2015. [Online]. Available: https://www.cs.cmu.edu/~rsalakhu/papers/oneshot1.pdf

[18] Z. Xu, Z. Shi, J. Wei, F. Mu, Y. Li, and Y. Liang, “Towards few-shot adaptation of foundation models via multitask finetuning,” *ICLR*, 2024. [Online]. Available: https://par.nsf.gov/biblio/10530266

[19] G. Han and S.-N. Lim, “Few-shot object detection with foundation models,” in *Proceedings of the IEEE/CVF Conference on Computer Vision and Pattern Recognition (CVPR)*, June 2024, pp. 28 608–28 618.

[20] X. Zheng, J. Chen, H. Wang, S. Zheng, and Y. Kong, “A deep learning-based approach for the automated surface inspection of copper clad laminate images,” *Applied intelligence*, vol. 51, pp. 1262–1279, 2021.

[21] P.-E. Josephson and Y. Hammarlund, “The causes and costs of defects in construction: A study of seven building projects,” *Automation in construction*, vol. 8, no. 6, pp. 681–687, 1999.

[22] S. Russell and P. Norvig, *Artificial Intelligence, Global Edition A Modern Approach*. Pearson Deutschland, 2021. [Online]. Available: https://elibrary.pearson.de/book/99.150005/9781292401171

[23] I. Goodfellow, Y. Bengio, A. Courville, and Y. Bengio, *Deep learning*. MIT press Cambridge, 2016, vol. 1, no. 2.

[24] A. Parnami and M. Lee, “Learning from few examples: A summary of approaches to few-shot learning,” *arXiv preprint arXiv:2203.04291*, 2022.

[25] J. Liang, H. Phan, and E. Benetos, “Learning from taxonomy: Multi-label few-shot classification for everyday sound recognition,” in *ICASSP 2024-2024 IEEE International Conference on Acoustics, Speech and Signal Processing (ICASSP)*. IEEE, 2024, pp. 771–775.

[26] J. Schmidhuber, “Evolutionary principles in self-referential learning,” *On learning how to learn: The meta-meta-... hook.) Diploma thesis, Institut f. Informatik, Tech. Univ. Munich*, vol. 1, no. 2, p. 48, 1987.

[27] T. Schaul and J. Schmidhuber, “Metalearning,” *Scholarpedia*, vol. 5, no. 6, p. 4650, 2010.

[28] S. Thrun and L. Pratt, “Learning to learn: Introduction and overview,” in *Learning to learn*. Springer, 1998, pp. 3–17.

[29] B. Kulis *et al.*, “Metric learning: A survey,” *Foundations and Trends® in Machine Learning*, vol. 5, no. 4, pp. 287–364, 2013.

[30] A. Santoro, S. Bartunov, M. Botvinick, D. Wierstra, and T. Lillicrap, “Meta-learning with memory-augmented neural networks,” in *International conference on machine learning*. PMLR, 2016, pp. 1842–1850.

[31] L. Torrey and J. Shavlik, “Transfer learning,” in *Handbook of research on machine learning applications and trends: algorithms, methods, and techniques*. IGI global, 2010, pp. 242–264.

[32] Z. Ji, X. Chai, Y. Yu, Y. Pang, and Z. Zhang, “Improved prototypical networks for few-shot learning,” *Pattern Recognition Letters*, vol. 140, pp. 81–87, 2020.

[33] A. Kruspe, “One-way prototypical networks,” *arXiv preprint arXiv:1906.00820*, 2019.

[34] H. Ismail Fawaz, G. Forestier, J. Weber, L. Idoumghar, and P.-A. Muller, “Deep learning for time series classification: a review,” *Data Mining and Knowledge Discovery*, vol. 33, no. 4, p. 917–963, Mar. 2019. [Online]. Available: http://dx.doi.org/10.1007/s10618-019-00619-1

[35] A. Krizhevsky, I. Sutskever, and G. E. Hinton, “Imagenet classification with deep convolutional neural networks,” in *Advances in Neural Information Processing Systems*, F. Pereira, C. Burges, L. Bottou, and K. Weinberger, Eds., vol. 25. Curran Associates, Inc., 2012. [Online]. Available: https://proceedings.neurips.cc/paper_files/paper/2012/file/c399862d3b9d6b76c8436e924a68c45b-Paper.pdf

[36] X. Wu and R. H. Chan, “Does meta-learning improve eeg motor imagery classification?” in *2022 44th Annual International Conference of the IEEE Engineering in Medicine & Biology Society (EMBC)*. IEEE, 2022, pp. 4048–4051.

[37] A. Nichol and J. Schulman, “Reptile: a scalable metalearning algorithm,” *arXiv preprint arXiv:1803.02999*, vol. 2, no. 3, p. 4, 2018.

[38] M. Tangermann, K.-R. Müller, A. Aertsen, N. Birbaumer, C. Braun, C. Brunner, R. Leeb, C. Mehring, K. J. Miller, G. R. Müller-Putz *et al.*, “Review of the bci competition iv,” *Frontiers in neuroscience*, vol. 6, p. 55, 2012.

[39] G. Schalk, D. J. McFarland, T. Hinterberger, N. Birbaumer, and J. R. Wolpaw, “Bci2000: a general-purpose brain-computer interface (bci) system,” *IEEE Transactions on biomedical engineering*, vol. 51, no. 6, pp. 1034–1043, 2004.

[40] X. Wang, A. Liu, L. Wu, C. Li, Y. Liu, and X. Chen, “A generalized zero-shot learning scheme for ssvep-based bci system,” *IEEE Transactions on Neural Systems and Rehabilitation Engineering*, vol. 31, pp. 863–874, 2023.

[41] O. Vinyals, C. Blundell, T. Lillicrap, k. kavukcuoglu, and D. Wierstra, “Matching networks for one shot learning,” in *Advances in Neural Information Processing Systems*, D. Lee, M. Sugiyama, U. Luxburg, I. Guyon, and R. Garnett, Eds., vol. 29. Curran Associates, Inc., 2016. [Online]. Available: https://proceedings.neurips.cc/paper_files/paper/2016/file/90e1357833654983612fb05e3ec9148c-Paper.pdf

[42] L. Sun, M. Zhang, B. Wang, and P. Tiwari, “Few-shot class-incremental learning for medical time series classification,” *IEEE Journal of Biomedical and Health Informatics*, vol. 28, no. 4, pp. 1872–1882, 2023.

[43] C. Papaioannou, E. Benetos, and A. Potamianos, “Lc-protonets: Multi-label few-shot learning for world music audio tagging,” *IEEE Open Journal of Signal Processing*, vol. 6, p. 138–146, 2025. [Online]. Available: http://dx.doi.org/10.1109/OJSP.2025.3529315

[44] M. P. Diwakar and B. Gupta, “Vggish deep learning model: Audio feature extraction and analysis,” in *International Conference on Data Management, Analytics & Innovation*. Springer, 2024, pp. 59–70.

[45] E. Law, K. West, M. I. Mandel, M. Bay, and J. S. Downie, “Evaluation of algorithms using games: The case of music tagging.” in *ISMIR*. Citeseer, 2009, pp. 387–392.

[46] M. Defferrard, K. Benzi, P. Vandergheynst, and X. Bresson, “Fma: A dataset for music analysis,” *arXiv preprint arXiv:1612.01840*, 2016.

[47] C. Papaioannou, I. Valiantzas, T. Giannakopoulos, M. Kaliakatsos-Papakostas, and A. Potamianos, “A dataset for greek traditional and folk music: Lyra,” *arXiv preprint arXiv:2211.11479*, 2022.

[48] M. K. Karaosmanoglu, “A turkish makam music symbolic database for music information retrieval: Symbtr.” in *ISMIR*, 2012, pp. 223–228.

[49] S. Gulati, J. Serrà Julià, K. K. Ganguli, S. Sentürk, and X. Serra, “Time-delayed melody surfaces for rāga recognition,” *International Society for Music Information Retrieval (ISMIR)*, 2016.

[50] S. Tam, M. Boukadoum, A. Campeau-Lecours, and B. Gosselin, “Siamese convolutional neural network and few-shot learning for embedded gesture recognition,” in *2022 20th IEEE Interregional NEWCAS Conference (NEWCAS)*. IEEE, 2022, pp. 114–118.

[51] E. Rahimian, S. Zabihi, A. Asif, S. F. Atashzar, and A. Mohammadi, “Few-shot learning for decoding surface electromyography for hand gesture recognition,” in *ICASSP 2021-2021 IEEE International Conference on Acoustics, Speech and Signal Processing (ICASSP)*. IEEE, 2021, pp. 1300–1304.

[52] N. Mishra, M. Rohaninejad, X. Chen, and P. Abbeel, “A simple neural attentive meta-learner,” *arXiv preprint arXiv:1707.03141*, 2017.

[53] M. Atzori, A. Gijsberts, C. Castellini, B. Caputo, A.-G. M. Hager, S. Elsig, G. Giatsidis, F. Bassetto, and H. Müller, “Electromyography data for non-invasive naturally-controlled robotic hand prostheses,” *Scientific data*, vol. 1, no. 1, pp. 1–13, 2014.

[54] X. S. Zhang, F. Tang, H. H. Dodge, J. Zhou, and F. Wang, “Metapred: Meta-learning for clinical risk prediction with limited patient electronic health records,” in *Proceedings of the 25th ACM SIGKDD international conference on knowledge discovery & data mining*, 2019, pp. 2487–2495.

[55] Y. Hu, R. Liu, X. Li, D. Chen, and Q. Hu, “Task-sequencing meta learning for intelligent few-shot fault diagnosis with limited data,” *IEEE Transactions on Industrial Informatics*, vol. 18, no. 6, pp. 3894–3904, 2021.

[56] H. Wang, X. Wang, Y. Yang, K. Gryllias, and Z. Liu, “A few-shot machinery fault diagnosis framework based on self-supervised signal representation learning,” *IEEE Transactions on Instrumentation and Measurement*, vol. 73, pp. 1–14, 2024.

[57] C. W. R. U. B. D. Center, “Seeded fault test data for condition monitoring of rolling element bearings,” https://csegroups.case.edu/bearingdatacenter/pages/download-data-file, 2019, accessed 2025-04-23.

[58] H. Wu and Y.-F. Li, “Wheel data,” 2023. [Online]. Available: https://dx.doi.org/10.21227/1v8x-s809

[59] Y. Wang, X. Chen, X. Gao, and S. Gao, “A benchmark dataset for ssvep-based brain–computer interfaces,” *IEEE Transactions on Neural Systems and Rehabilitation Engineering*, vol. 25, no. 10, pp. 1746–1752, 2016.

[60] B. Liu, X. Huang, Y. Wang, X. Chen, and X. Gao, “Beta: A large benchmark database toward ssvep-bci application,” *Frontiers in neuroscience*, vol. 14, p. 627, 2020.

[61] A. L. Goldberger, L. A. Amaral, L. Glass, J. M. Hausdorff, P. C. Ivanov, R. G. Mark, J. E. Mietus, G. B. Moody, C.-K. Peng, and H. E. Stanley, “Physiobank, physiotoolkit, and physionet: components of a new research resource for complex physiologic signals,” *circulation*, vol. 101, no. 23, pp. e215–e220, 2000.

[62] H. A. Dau, A. Bagnall, K. Kamgar, C.-C. M. Yeh, Y. Zhu, S. Gharghabi, C. A. Ratanamahatana, and E. Keogh, “The ucr time series archive,” *IEEE/CAA Journal of Automatica Sinica*, vol. 6, no. 6, pp. 1293–1305, 2019.

[63] K. Simonyan and A. Zisserman, “Very deep convolutional networks for large-scale image recognition,” *arXiv preprint arXiv:1409.1556*, 2014.

[64] K. He, X. Zhang, S. Ren, and J. Sun, “Deep residual learning for image recognition,” in *Proceedings of the IEEE conference on computer vision and pattern recognition*, 2016, pp. 770–778.

[65] J. Paulus, “Optimization and evaluation of deep learning methods for monitoring screw-fastening processes in the final assembly of electric drives,” Master thesis, Friedrich-Alexander-Universität Erlangen-Nürnberg, Erlangen, Germany, 2024.

[66] DEPRAG SCHULZ GMBH u. CO., “Minimat-ec,” https://www.deprag.com/fileadmin/bilder_content/emedia/broschueren_pics/emedia_schraubtechnik/D3490/D3490de.pdf, 2022, zugriff am: 16. Januar 2023.

[67] S. M. R. Arnold, P. Mahajan, D. Datta, I. Bunner, and K. S. Zarkias, “learn2learn: A library for meta-learning research,” *CoRR*, vol. abs/2008.12284, 2020. [Online]. Available: https://arxiv.org/abs/2008.12284

[68] W. Li, Z. Wang, X. Yang, C. Dong, P. Tian, T. Qin, H. Jing, Y. Shi, L. Wang, Y. Gao, and J. Luo, “Libfewshot: A comprehensive library for few-shot learning,” *IEEE Transactions on Pattern Analysis & Machine Intelligence*, no. 01, pp. 1–18, 2023.

[69] W. Thomala and K.-H. Kloos, *Schraubenverbindungen*, 5th ed. Springer Berlin, Heidelberg, 2007, originally published under Wiegand, H. in the series: Konstruktionsbücher. Part of the eBook package: Computer Science and Engineering (German Language).

[70] Outcast, “Transform multi-label problem to multi-class problem,” Data Science Stack Exchange, https://datascience.stackexchange.com/questions/56170/transform-multi-label-problem-to-multi-class-problem, July 2019, modified July 23, 2019; accessed April 25, 2025.

[71] Wikipedia contributors, “Power set,” https://en.wikipedia.org/wiki/Power_set#cite_note-FOOTNOTEPuntambekar20071-2-4, 2025, [Online; accessed 25 April 2025].

[72] P. Dixit, “Why is odd sized kernel preferred over even sized kernel?” Aug 2021, accessed: 13 April 2025. [Online]. Available: https://medium.com/geekculture/why-is-odd-sized-kernel-preferred-over-even-sized-kernel-a767e47b1d77

[73] A. Vaswani, N. Shazeer, N. Parmar, J. Uszkoreit, L. Jones, A. N. Gomez, Ł. Kaiser, and I. Polosukhin, “Attention is all you need,” *Advances in neural information processing systems*, vol. 30, 2017.

[74] AutonLab, “MOMENT-1-large model configuration (config.json),” https://huggingface.co/AutonLab/MOMENT-1-large/blob/main/config.json, 2024, hugging Face repository, commit a0bebe9; accessed 27 Apr 2025.

[75] E. J. Hu, Y. Shen, P. Wallis, Z. Allen-Zhu, Y. Li, S. Wang, L. Wang, W. Chen *et al.*, “Lora: Low-rank adaptation of large language models.” *ICLR*, vol. 1, no. 2, p. 3, 2022.

[76] M. Goswami, K. Szafer, A. Choudhry, Y. Cai, S. Li, and A. Dubrawski, “Moment forecasting tutorial notebook,” https://github.com/moment-timeseries-foundation-model/moment/blob/main/tutorials/forecasting.ipynb, 2024, jupyter notebook, commit cd889e0 (03 Oct 2024). Accessed 28 Apr 2025.

[77] H. Zhou, S. Zhang, J. Peng, S. Zhang, J. Li, H. Xiong, and W. Zhang, “Informer: Beyond efficient transformer for long sequence time-series forecasting,” in *The Thirty-Fifth AAAI*

Conference on Artificial Intelligence, AAAI 2021, Virtual Conference, vol. 35, no. 12. AAAI Press, 2021, pp. 11 106–11 115.

[78] C. M. Bishop, *Neural networks for pattern recognition*. Oxford university press, 1995.

[79] E. Triantafillou, T. Zhu, V. Dumoulin, P. Lamblin, U. Evci, K. Xu, R. Goroshin, C. Gelada, K. Swersky, P.-A. Manzagol *et al.*, "Meta-dataset: A dataset of datasets for learning to learn from few examples," *arXiv preprint arXiv:1903.03096*, 2019.

[80] J. He, R. Hong, X. Liu, M. Xu, Z.-J. Zha, and M. Wang, "Memory-augmented relation network for few-shot learning," in *Proceedings of the 28th ACM International Conference on Multimedia*, 2020, pp. 1236–1244.

[81] N. Houlsby, A. Giurgiu, S. Jastrzebski, B. Morrone, Q. De Laroussilhe, A. Gesmundo, M. Attariyan, and S. Gelly, "Parameter-efficient transfer learning for NLP," in *Proceedings of the 36th International Conference on Machine Learning*, ser. Proceedings of Machine Learning Research, K. Chaudhuri and R. Salakhutdinov, Eds., vol. 97. PMLR, 09–15 Jun 2019, pp. 2790–2799. [Online]. Available: https://proceedings.mlr.press/v97/houlsby19a.html

A Appendix

Table A.11: 1D CNN hyperparameters

Hyperparameters	Range
number of convolution block	[2,6]
number of kernels each convolution block	[16,64]
kernel size each convolution block	[2,8]
convolution activation function	{Relu, Selu, Elu, mish}
pooling function	{Max,Avg}
pooling kernel size each convolution block	[2,4]
number of linear layers in dense block	[1,3]
number of features each linear layer	[64,256]
activation function in linear layers	{Relu, Selu, Elu, mish}

Table A.12: InceptionTime hyperparameters

Hyperparameters	Range
representation dimensions	[64,256]
number of filters in convolution layer	[4,16]
number of inception modules	[2,5]
number of linear layers in dense block	[1,3]
number of features each linear layer	[64,256]
activation function in linear layers	{Relu, Selu, Elu, mish}

Table A.13: Moment Lora hyperparameters

Hyperparameters	Range
Lora alpha	[4,8]
Lora rank	[4,16]
Lora target	{{q}, {v}, {q,v}}

Table A.14: Moment linear hyperparameters

Hyperparameters	Range
number of linear layers in dense block	[1,3]
number of features each linear layer	[64,256]
activation function in linear layers	{Relu, Selu, Elu, mish}

Table A.15: Moment lora + linear hyperparameters

Hyperparameters	Range
Lora alpha	[4,8]
Lora rank	[4,16]
Lora target	{{q}, {v}, {q,v}}
number of linear layers in dense block	[1,3]
number of features each linear layer	[64,256]
activation function in linear layers	{Relu, Selu, Elu, mish}